

Doppler Lidar–Based Wind-Profile Measurement System for Offshore Wind-Energy and Other Marine Boundary Layer Applications

YELENA L. PICHUGINA

Cooperative Institute for Research in Environmental Sciences, and NOAA/Earth System Research Laboratory, Boulder, Colorado

ROBERT M. BANTA, W. ALAN BREWER, SCOTT P. SANDBERG, AND R. MICHAEL HARDESTY

NOAA/Earth System Research Laboratory, Boulder, Colorado

(Manuscript received 15 February 2011, in final form 9 September 2011)

ABSTRACT

Accurate measurement of wind speed profiles aloft in the marine boundary layer is a difficult challenge. The development of offshore wind energy requires accurate information on wind speeds above the surface at least at the levels occupied by turbine blades. Few measured data are available at these heights, and the temporal and spatial behavior of near-surface winds is often unrepresentative of that at the required heights. As a consequence, numerical model data, another potential source of information, are essentially unverified at these levels of the atmosphere. In this paper, a motion-compensated, high-resolution Doppler lidar–based wind measurement system that is capable of providing needed information on offshore winds at several heights is described. The system has been evaluated and verified in several ways. A sampling of data from the 2004 New England Air Quality Study shows the kind of analyses and information available. Examples include time–height cross sections, time series, profiles, and distributions of quantities such as winds and shear. These analyses show that there is strong spatial and temporal variability associated with the wind field in the marine boundary layer. Winds near the coast show diurnal variations, and frequent occurrences of low-level jets are evident, especially during nocturnal periods. Persistent patterns of spatial variability in the flow field that are due to coastal irregularities should be of particular concern for wind-energy planning, because they affect the representativeness of fixed-location measurements and imply that some areas would be favored for wind-energy production whereas others would not.

1. Introduction

High-quality, trustworthy measurements of wind speed profiles through the lowest several hundred meters of the atmosphere are an important but difficult challenge over the ocean. Obtaining offshore anemometer data at these heights, for example, would require deployment of expensive tall towers. Remote sensors, such as radar, sodar, or lidar, can provide such profiles, and operation from fixed platforms should yield performance that is comparable to that obtained on land. Construction of fixed platforms is likely to be prohibitively expensive, however. Although use of existing fixed platforms can be an option, the location may not be desirable. Profiling remote

sensors may also be mounted on portable floating platforms, such as ships or buoys, which can then be sited in more suitable locations, but significant technological obstacles are associated with removing ocean wave–induced motions and other platform motions from the desired measurements of the airflow. Removal of these unwanted accelerations is necessary to produce accurate estimates of wind speed and direction. Here, we describe a motion-compensating, scanning Doppler lidar–based wind measurement system that is capable of producing reliable vertical profiles of marine wind speed and direction from shipboard at high resolution (<10 m). The light detection and ranging (lidar) system was developed and operated by the National Oceanic and Atmospheric Administration (NOAA) Earth System Research Laboratory (ESRL). Here we present comparisons with more conventional measurement systems, such as rawinsondes, and we offer examples of the kind of data available from this system.

Corresponding author address: Yelena L. Pichugina, University of Colorado at Boulder, Cooperative Institute for Research in Environmental Sciences, 385 Broadway, Boulder, CO 80305-3337.
E-mail: yelena.pichugina@noaa.gov

One industry that urgently needs any available morsel of reliable wind-profile information in the marine environment is the wind-energy (WE) industry. It has been estimated that wind resources off the coasts of the United States can provide more “than 4,000 GW, or roughly four times the generating capacity currently carried on the U.S. electric grid” (Musial and Ram 2010). The first U.S. offshore wind farm of 130 turbines will supply about 75% of the electricity consumed by Cape Cod residents at a cost of more than \$2 billion (Lindsay 2010). The development of offshore WE offers many advantages as compared with inland wind projects but also has drawbacks, as summarized by Musial and Butterfield (2004) and Musial and Ram (2010). Most disadvantages stem from inaccessibility and the much harsher marine environment, requiring higher investment, installation, and maintenance costs. Larger, more-cost-effective turbines can be installed offshore, however, because of the ability to transport larger hardware components to chosen sites. Other advantages listed include reduced transmission costs because of the closer location of wind farms to large load centers on the East Coast, minimal visual impact for wind farms sited more than a few miles from the shore, and presumed stronger marine winds that are also presumed to be less turbulent.

The meteorological challenge in the coastal zone and farther offshore is that these winds are driven by many different scales of forcing. Synoptic-scale midlatitude storms can produce strong winds that often intensify as they move offshore. Tropical storms and hurricanes can also produce wind speed extremes. As a result of roughness and thermal contrasts between land and water, offshore flow generates transitional or “internal” boundary layer structures that produce changes in wind speeds with distance from the coastline but are not well understood. The diurnal heating cycle produces sea-breeze circulations that change over periods of a few hours, and diurnally varying low-level jets (LLJ) have often been observed in available offshore wind profiles. The interaction of these processes with onshore topography or irregular coastlines adds further complexity to the horizontal and vertical structures of the flows offshore. All of these factors can produce strong spatial and temporal variability in the offshore wind field; examples of such variations as observed by the NOAA/ESRL Doppler lidar system will be presented.

A major obstacle to offshore WE development is the lack of reliable wind measurements aloft, because of the difficulties mentioned above. High-precision data are needed to advance turbine engineering and installation design technologies as well as to provide accurate assessments of wind resources (wind speeds) and other properties of the flow at turbine-rotor heights. Such assessments

will be needed for success in wind-farm development and operations (Schreck et al. 2008). A potentially important tool in providing offshore winds aloft is the numerical weather prediction (NWP) model, but, without measurements at turbine-blade levels for verification, the accuracy and fidelity of model output are unknown. In a recent study that compared annually averaged wind speed forecast errors from a global model with data from two offshore wind towers on fixed platforms reaching 70 and 100 m above sea level, Drechsel et al. (2011, manuscript submitted to *J. Appl. Meteor. Climatol.*) found model errors of 1–2 m s⁻¹ and relative errors of 15%–20%, depending on the model-derived variable used for comparison. Comparisons with turbine-nacelle winds, which were available for this study, yielded poorer results, as expected. More such studies are needed.

To address the need for offshore wind measurements aloft at turbine-rotor heights, remote sensing instrumentation is an option. Doppler lidars, for example, are able to provide high-quality measurements of wind and turbulence profiles from the surface up to several hundred meters above the air–water interface (Kindler et al. 2007; Peña et al. 2008, 2009; Mann et al. 2010; Pichugina et al. 2010). NOAA researchers have used Doppler lidar systems extensively on land and at sea during the past two decades to provide high-resolution profiles of wind speed, wind direction, and turbulence. At sea, these systems have been deployed on ships during several research campaigns (e.g., Wulfmeyer and Janjić 2005; Tucker et al. 2009, 2010; Pichugina et al. 2010), as shown in Table 1. For such marine operations, the lidar is installed in a “seatainer” together with a GPS-based inertial navigation unit (INU) capable of determining platform motion and orientation. A hemispheric (azimuth–elevation) scanner, mounted onto the roof of the seatainer, is controlled to compensate for pointing errors introduced by platform motion, including those induced by ocean waves (Fig. 1). Studies on land using NOAA’s High-Resolution Doppler Lidar (HRDL) have demonstrated the ability of this instrument to reveal the structure and evolution of boundary layer processes up to several hundred meters above the ground at fine vertical, horizontal, and temporal resolutions (Banta et al. 2002, 2003, 2006; Pichugina et al. 2008, 2010). These high-quality measurements are in precisely the layer of the atmosphere for which information is most needed by the WE industry (Emeis et al. 2007, Kindler et al. 2007).

To demonstrate the ability of shipborne Doppler lidar to provide high-quality measurements in the marine boundary layer (MBL), this paper will present examples of analysis products obtained from HRDL measurements during the New England Air Quality Study (NEAQS) in the summer of 2004 (e.g., Darby et al. 2007; Angevine et al. 2006; White et al. 2007). Section 2 contains brief

TABLE 1. List of previous field experiments at sea involving Doppler lidar measurements of atmospheric wind speed, wind direction, and turbulence properties.

Year	Month	Expt	Instrument	Place	Platform
1995	Apr	Marine Boundary Layer Experiment (MBLEX)	HRDL	Monterrey, CA	Ground
1999	Jul	Nauru-99	HRDL	Pacific Ocean	Ship based
2000	May	Creates Havoc	HRDL	Bahamas	Ship based
2001	Sep	East Pacific Investigation of Climate (EPIC)	MOPA	Southeastern Pacific	Ship based
2004	Jul	NEAQS-04	HRDL	New England	Ship based
2004	Jul	Close Connection	MOPA	Bahamas	Ship based
2005	May	Environmental Mapping and Monitoring with Airborne Laser and Digital Images (EMMA)	MOPA	Bermuda	Ship based
2005	Jan	Rain in Cumulus over the Ocean (RICO)	MOPA	Barbuda	Ship based
2006	Jul	Texas Air Quality Study (TexAQS)	HRDL	Houston, TX	Ship based
2008	Oct	Variability of the American Monsoon Systems (VAMOS) Ocean-Cloud-Atmosphere-Land Study (VOCALS)	HRDL	Southeastern Pacific	Ship based

descriptions of the lidar and motion-compensation systems, a review of verification studies, and a discussion of the NEAQS lidar dataset. Section 3 presents several examples of the vertical, horizontal, and time-evolving structures of the wind profiles; time series of wind speed and direction at several vertical levels across the atmospheric layer occupied by turbine blades; and examples of distributions of wind speed and direction for two nighttime periods. Section 4 contains examples of how the dataset can be used to form longer-term averages, including monthly distributions and averages of wind speed and shear, and their diurnal variation. Section 5 contains conclusions and recommendations.

2. Offshore measurements of winds aloft

HRDL, the Doppler lidar used in this study, is a scanning, coherent, pulsed Doppler lidar that was designed for atmospheric boundary layer research, as described by Grund et al. (2001) and Wulfmeyer et al. (2000). It is similar in concept to Doppler weather radar, although the scattering targets for its near-IR signal are aerosol particles rather than hydrometeors. This makes the lidar useful for mapping the wind field in clear air, since aerosol particles are widely distributed in the lowest 2–4 km of the atmosphere and near the ocean surface salt particles are especially effective backscatter targets. HRDL provides range-resolved measurements of the radial or “line of sight” wind, that is, the component of the velocity parallel to the beam, and aerosol backscatter, at a range resolution of 30 m. The minimum range of the instrument along the beam is <200 m. The other Doppler lidar used during shipboard operations was NOAA/ESRL’s miniature Master-Oscillator/Power-Amplifier (mini MOPA) system. Technical attributes of these lidar systems are given in Table 2. Both systems

employ a well-collimated optical beam, and so they do not suffer from sidelobe contamination. During NEAQS the HRDL, deployed on board the NOAA Research Vessel *Ronald H. Brown* (*RHB*), operated in a continuous measurement mode from 9 July through 12 August 2004, with occasional interruptions occurring during heavy-rain and dense-fog episodes.



FIG. 1. (top) Instrumentation deployed on the *RHB*, including the lidar seatainer. (bottom) Doppler lidar scanner (left part of photograph), probing the atmosphere in the conical scan mode, and GPS housing (bottom-right part of photograph).

TABLE 2. Technical characteristics of NOAA/ESRL Doppler lidars.

Characteristics	Mini MOPA	HRDL
Wavelength	9.2–11.3 μm	2.02 μm
Pulse energy	1.5 mJ	2.0 mJ
Pulse rate	300 Hz	200 Hz
Range resolution	60 m	30 m
Velocity resolution	$\sim 50 \text{ cm s}^{-1}$	$\sim 10 \text{ cm s}^{-1}$
Time resolution	0.3 s	0.5 s
Min range	90 m	189 m
Max range	5–12 km	3–8 km
Beamwidth range	6–28 cm	

a. Scanning

The HRDL system includes full scanning capability in azimuth and elevation (Fig. 2), which we will refer to as hemispheric, even though HRDL's ability to operate at negative elevation angles makes the coverage greater than a hemisphere. On the ship, the signal was blocked at certain azimuths by the ship superstructure, but this is not a significant limitation in obtaining accurate profile data from the velocity–azimuth–display (VAD) wind-calculation technique used, because the blocked sector is less than 50° of azimuth. The lidar scanning strategy during NEAQS included sweeps along both constant azimuth and constant elevation angles to provide a variety of high-resolution boundary layer information

(Fig. 2). Individual lidar scans can produce sometimes-dramatic images that provide critical clues in the interpretation of the dataset, for example the Kelvin–Helmholtz wave images of Newsom and Banta (2003) and the gust-front analysis of Darby et al. (2002). The current study, however, makes use of the ability to process the scan data into high-resolution profiles of the mean wind speed and direction averaged over time intervals of interest. Accurate profiles can be achieved for intervals as short as from 30 s to 2 min, depending on the scans employed (Pichugina et al. 2008), but for this study profiles will be compiled for 15-min averages, because the scanning sequences used were in 15-min blocks [as also during the 2006 Texas Air Quality Study; Tucker et al. (2009, 2010)].

The current study makes use of conical scanning (Fig. 2, bottom left) and the VAD analysis procedure. The original VAD technique described by Lhermitte and Atlas (1961) and Browning and Wexler (1968) is based on individual conical scans (Fig. 2, bottom left), in which the lidar (or radar) beam sweeps the atmosphere in azimuth from 0° to 360° at a fixed elevation angle, usually completed in ~ 2 min. These scans at small elevation angles produce shallow profiles having high vertical resolution, whereas such scans at larger elevation angles produce deeper profiles but at coarser vertical spacing. Shallow conical scans can provide vertical

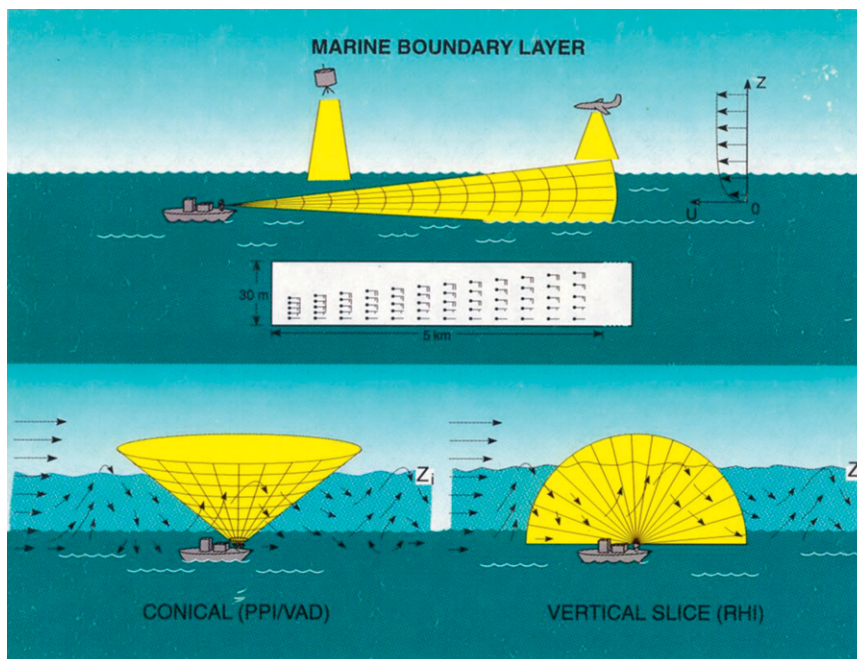


FIG. 2. Common scanning patterns used by HRDL: (top) elevation sector or “vertical slice” scan, (bottom left) azimuth or conical scan at a fixed elevation angle, and (bottom right) full 180° elevation vertical-slice scan.

resolutions of <5 m in the lowest ~ 100 m of the MBL, with the lowest measurement within a few meters of the scanner height. This procedure repeated at multiple elevation angles produces concentric cones of data for computing vertical profiles of the horizontal wind components through a deep layer; for example, a sequence of 1° -, 2° -, 10° -elevation scans was often used during NEAQS. Another technique, using data from HRDL elevation (or vertical slice) sector scans (Fig. 2, top), has also been used to calculate profiles of mean winds and turbulent velocity variances for one (Pichugina et al. 2008) or both (Tucker et al. 2009) horizontal wind components, but this approach is not used in this paper.

We employed a modified form of the VAD technique, designed to allow all scans in the averaging interval to be used in the mean-profile calculation (Banta et al. 2002). Here, we present results from wind speed and direction profiles obtained by averaging scan data over 15-min intervals (to match the scan-sequence repetition cycle) using the modified VAD procedure. Analyses presented here use only the conical scans, and so occasional gaps appear in the cross sections when other scans (e.g., elevation or staring) were being performed over the entire 15-min period. For further analysis these data are then averaged over diurnal and monthly periods to obtain statistical information such as distributions and mean parameters.

b. Motion compensation system

HRDL's operation from a ship-based platform had to address many challenges, such as a constantly accelerating reference frame and vibration from ship engines. A major obstacle to obtaining accurate wind profiles from the high-precision lidar measurements using these techniques is compensating for the pointing error and along-beam platform velocity that are due to ship motions, including those induced by wave action. To accomplish this, the lidar is equipped with a system that 1) determines the orientation and motion of the platform and then actively stabilizes the pointing of the scanner and 2) corrects the lidar velocity measurement by estimating and removing the platform motion component along the lidar pointing direction.

This motion-compensation system consists of a GPS-based INU, rigidly mounted to the seatainer, and a high-rate six-axis accelerometer mounted near the base of the hemispheric scanner. The angular rates and linear accelerations measured by the accelerometer are integrated in time to determine the angular orientation and linear motion of the platform several hundred times per second. Information from the lower-rate GPS INU is used to remove the effect of drift in the accelerometer measurement. Angular motion and orientation information are

provided at a rate of 50 Hz to the control computer that drives the scanner so as to maintain its pointing direction in the Earth-based reference frame (the "world frame" of reference) according to the chosen scan parameters.

Several tests are used to determine the accuracy of the pointing-angle corrections. In one, the pointing correction is evaluated at sea by performing an azimuth scan at a low elevation angle (e.g., 0.5°) and then using a boresighted video camera to determine the pointing error relative to the horizon (Fig. 3, top right). In a second test, the scanner can be actively stabilized while pointed at the sun. Inspection of the boresighted crosshairs relative to the solar disk provides an estimate of pointing accuracy (Fig. 3, bottom right). The pointing accuracy of the motion-compensation system is limited by the long-term stability of the GPS INU. These tests indicated that during NEAQS the development and implementation of the real-time motion-compensation system allowed maintaining the chosen scan parameters in the world frame to within $\sim 1^\circ$ or so under conditions normally encountered. For more recent deployments, installation of a more stable and precise INU and other improvements have allowed compensation for the ship's motions to within 0.5° .

The estimate of the platform's linear motion is combined with the scanner's world-frame pointing angles to determine the motion of the platform along the line of sight (LOS) of the lidar measurement. Two tests to assess the accuracy of the LOS platform velocity correction are to measure the velocity of stationary hard targets while the ship is under way and to compare the lidar-derived wind profiles with profiles measured by other means. For the first test, a series of low-elevation-angle azimuth scans was performed over a 3-h period as the ship was approaching a harbor. The random noise introduced to each LOS velocity measurement due to platform motion correction was 30 cm s^{-1} . By averaging these LOS estimates of the stationary-target motion over 3 min, the mean calculated motion was $5.3 \pm 1.5 \text{ cm s}^{-1}$ —very close to the actual zero motion of the targets. Results from the second types of test, comparisons with other instrumentation, are presented in the next section.

c. Lidar data validation

A critical issue for WE applications is the question of measurement accuracy of the instruments employed, yet few careful studies have documented the accuracy of remote sensing and other methods used to determine winds aloft. A few studies in Europe have compared wind speed data from a continuous-wave scanning Doppler lidar with data from nearby towers (with offshore heights up to 100 m) instrumented with cup anemometers at both inland sites and on an offshore fixed platform

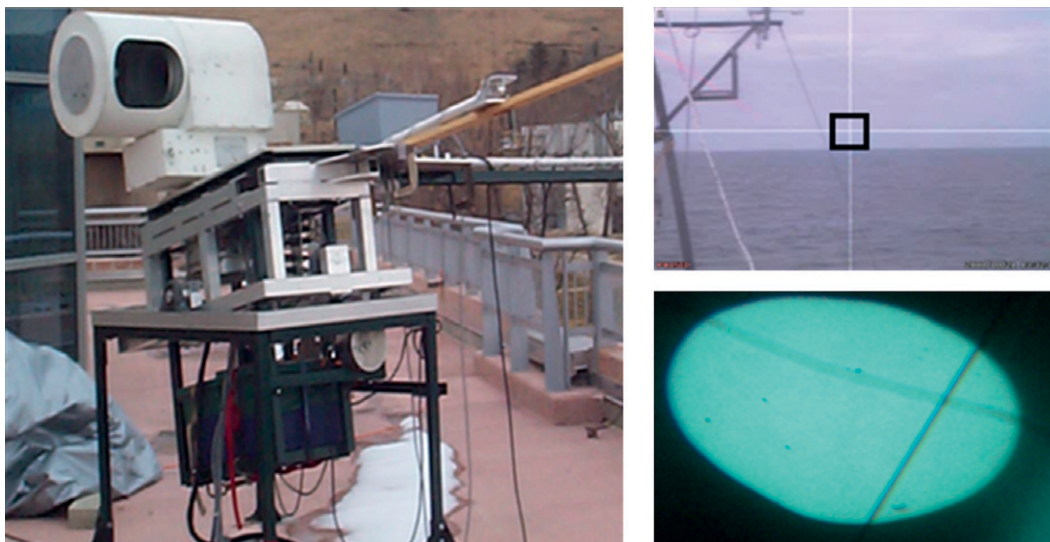


FIG. 3. (left) The triple-swiveling motorized platform used to simulate roll, pitch, and yaw of ship motions during pointing-angle accuracy tests on the porch of the NOAA laboratory. (top right) Boresighted crosshairs while performing azimuth scans at $\frac{1}{2}^\circ$ elevation. Dimensions of the square box superimposed on the image are equivalent to 1° of arc on a side, so that the lower side of the box should skim the horizon during the scan. (bottom right) Projection of solar disk with boresighted crosshairs while actively pointing at the center of the sun. Diameter of the solar disk subtends an angle of very nearly 0.5° so that a crosshair image remaining within the solar disk implies a pointing-angle accuracy of better than $\frac{1}{2}^\circ$.

(Smith et al. 2006; Kindler et al. 2007; Peña et al. 2008, 2009; Mann et al. 2010). These studies found high correlation coefficients ($r^2 \geq 0.99$) between the lidar and anemometer winds for 10-min averages, providing evidence that Doppler lidar can be a very precise wind-measuring instrument.

In this section we review some studies that have compared pulsed, scanning Doppler lidar measurements on land and at sea with more familiar sensors, including tower-mounted anemometers, sodars, and rawinsondes. One approach to assessing HRDL performance versus tower-mounted anemometer data is to operate the lidar in staring mode with the beam aimed at a sonic anemometer and to compare the 2-Hz individual-beam velocity estimates for the appropriate lidar range gate with “instantaneous” tower values. Kelley et al. (2007) found good agreement between HRDL and sonic measurements on a 120-m tower but also noted a systematic tendency for sonic-measured winds to be weaker than lidar winds at slow wind speeds and higher than lidar wind speeds at stronger wind speeds. They attributed this to Reynolds number–dependent tower flow-distortion effects in the sonic-measured winds, which existed even though periods during which the anemometer boom was downwind of the tower structure were excluded from the analysis.

For WE applications the quantities of greatest interest are mean winds averaged over time intervals of

several minutes. Such averaging considerably improves the achievable instrument measurement precision. For example, using a 1983 version of NOAA’s carbon dioxide Doppler lidar on land, Hall et al. (1984) estimated the rms random instrumental-error contribution for a single VAD scan—consisting of 304 beams around the sampling ring and taking 2–3 min to complete—at $6\text{--}15\text{ cm s}^{-1}$. Pichugina et al. (2008) showed that HRDL wind speed data averaged over 5–15-min intervals were highly correlated with sonic-anemometer means for the same vertical level and averaging period (Fig. 4, top panels), as indicated by correlation coefficients r of >0.95 for the entire sample and r of >0.98 for many individual nights. Banakh et al. (2010) have also shown that estimates of the wind velocity and wind direction could be obtained with acceptable accuracy even at low signal-to-noise ratios (down to -22 dB for their application). HRDL and sodar velocities were compared and were found to be mostly in good agreement within the turbulent nocturnal BL, the layer in which the sodar signal was generally strong enough to obtain good velocity estimates (Pichugina et al. 2008). Overall, these comparisons demonstrate HRDL’s ability to provide accurate estimates of spatially and temporally averaged *mean* wind speed in regions of sufficiently high aerosol backscatter signal, which is routinely observed in at least the lowest 500 m of the atmosphere during fog- and cloud-free conditions. These studies have also documented the

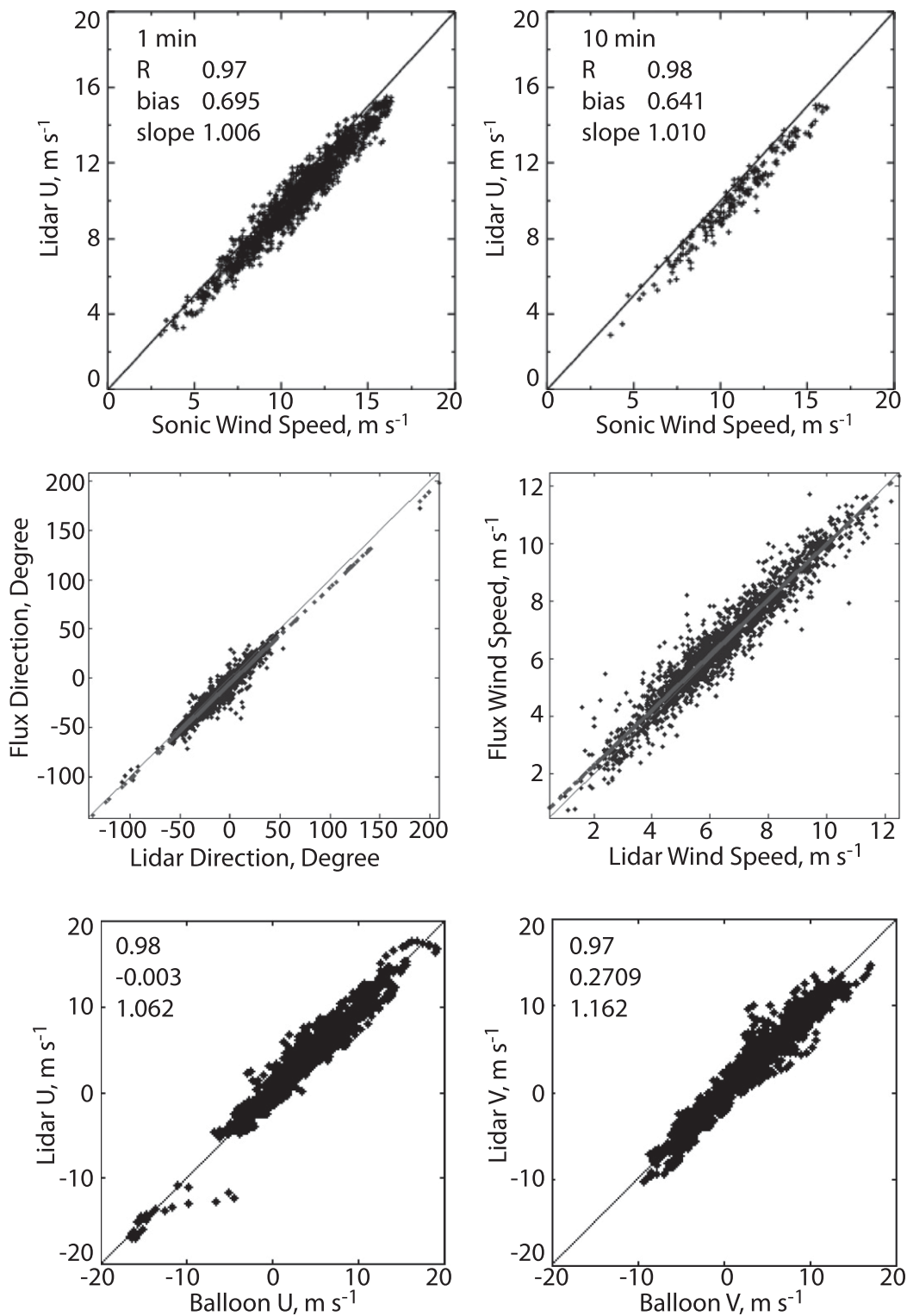


FIG. 4. Scatter diagrams showing comparisons between (top) ground-based HRDL (horizontal axis; m s⁻¹) and sonic-anemometer measurements (vertical axis; m s⁻¹) from 54-, 67-, 85-, and 116-m tower levels over land, (middle) shipboard HRDL-measured wind (left) direction and (right) speed and motion-compensated, sonic-anemometer “flux winds” at 17 m (Fairall et al. 2006), and (bottom) ship-based HRDL (vertical axis) and rawinsonde (horizontal axis) (left) *U* and (right) *V* components (Wolfe et al. 2007).

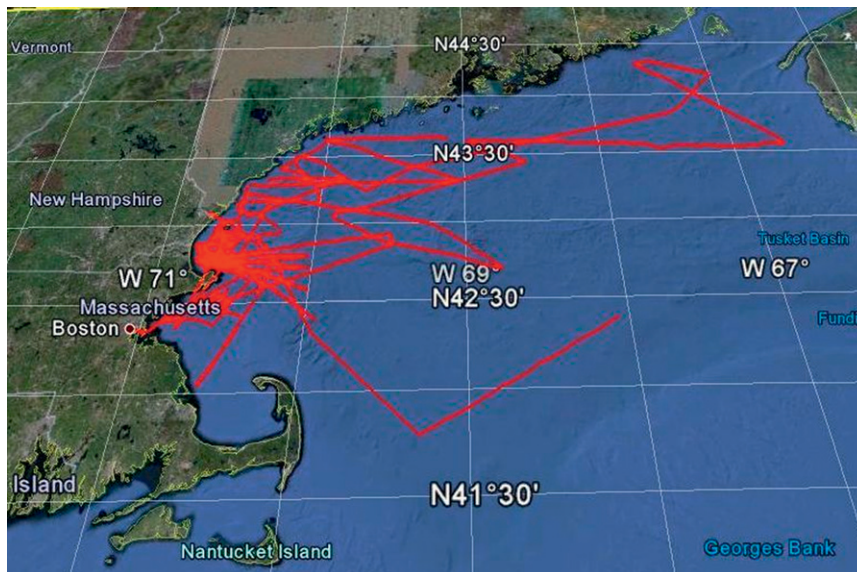


FIG. 5. Ship tracks during the 331 h of HRDL measurements in July 2004. [U.S. Dept. of State Geographer, ©2011 Europa Technologies, Data Scripps Institution of Oceanography (SIO), NOAA, U.S. Navy, National Geospatial-Intelligence Agency (NGA), General Bathymetric Chart of the Oceans (GEBCO), ©2011 Google.]

ability of HRDL to measure turbulence variables, including streamwise (along wind) variance profiles (Pichugina et al. 2008; Drobinski et al. 2004) and turbulence kinetic energy dissipation (Banakh et al. 2010).

Although a lidar system may be capable of high-precision measurements over land, the important question for offshore wind measurements is how well the lidar system can measure mean-wind components over the ocean from a ship or buoy platform. At present this question cannot be addressed as well at sea as over land because of the absence of offshore tower or other solid-platform measurements.

For the HRDL system the stationary hard-target tests indicated a precision of $<10 \text{ cm s}^{-1}$ for the motion-compensation calculation. Comparisons have been made with shipborne sonic-anemometer measurements from a boom ahead of the bow at a height of 17 m above the ocean surface. The anemometer was also effectively compensated for ship motions, as described by Fairall et al. (2006). The results of the comparisons show that HRDL winds at low elevation angles, evaluated at 17 m, agree well with the sonic-anemometer winds (Fig. 4, middle panels).

Other comparisons with rawinsondes and radar wind profilers at sea have been reported by Wolfe et al. (2007). HRDL and the rawinsonde winds agreed well as shown in Fig. 4 (bottom panels) for all vertical levels that were compared. HRDL winds were also in reasonable agreement with profiler wind speeds at heights of $>\sim 500 \text{ m}$ above the sea surface. Below this level, profiler winds often deviated significantly from HRDL and rawinsondes, which

was attributed to the radar sidelobe signal reflecting from moving ocean waves, sometimes referred to as “sea clutter” (Wolfe et al. 2007). Over land, rawinsonde winds have an uncertainty of $\sim 1 \text{ m s}^{-1}$ or more (a factor of at least 5–10 greater than HRDL), which should not be affected by launch from a ship, once the balloon rises above the ship’s atmospheric wake (which may extend up to 60–80 m). The agreement between HRDL and rawinsonde thus indicates that the uncertainty in the HRDL shipboard winds should be at least this good. Although WE applications require better precision, the level of precision in the mean HRDL winds demonstrated by these tests is at least sufficient to explore spatial and temporal variability of the offshore winds and the vertical structure of offshore wind profiles.

A preliminary error-propagation analysis of the random instrumental errors and those due to the motion-compensation system predicts a precision of $<10 \text{ cm s}^{-1}$ for 15-min-averaged HRDL wind estimates. Further work is needed, perhaps involving comparisons with lidars or tall towers mounted on a fixed offshore platform, to establish how closely the shipboard HRDL system approximates the high precision that is obtainable during land-based operations.

d. NEAQS dataset

Figure 5 illustrates all ship tracks in July 2004, when 155 nighttime (0000–1200 UTC) and 176 daytime (1200–0000 UTC) hours of HRDL measurements were taken at distances of 0.42 to 292 km from the coast. Because

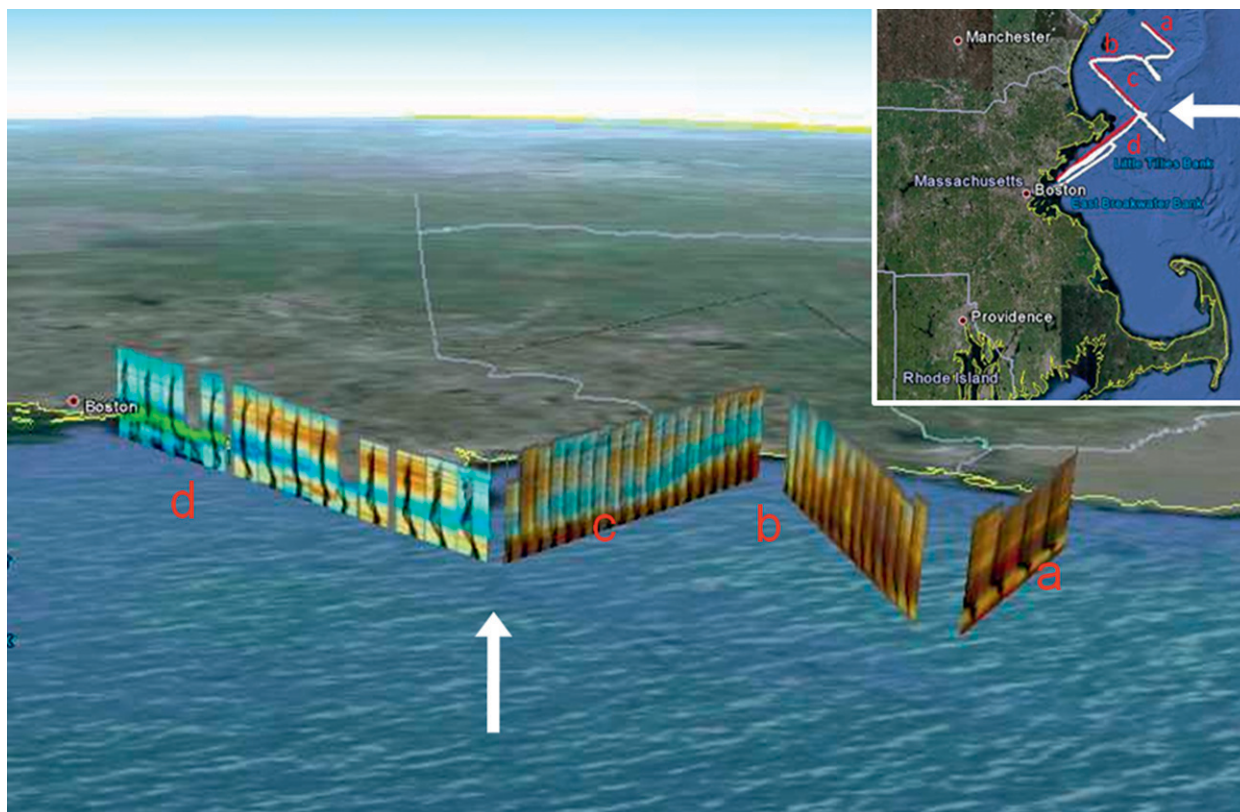


FIG. 6. Time–height cross sections of color-coded wind speed for four segments of the ship track on 21 Jul 2004, superimposed on a Google-Earth image of the Gulf of Maine region looking toward the west. Color coding of the wind speed (see Fig. 7) runs from 0 (green) to 10 (red) m s^{-1} , and 15-min wind speed profiles are shown from 10 to 1500 m above the water surface. Insert shows the locations of the four ship-track segments, plotted on an image of the New England coastline, where north is up and the white arrow indicates the point of view. The image provides an overview of the spatial and temporal variability of the wind along the track. A more detailed view of the data for the entire day and the color bar for the wind speeds is provided in Fig. 7, below. Time periods of the four segments are 0002:59–0132:58 UTC for segment a, 0147:58–0533:00 UTC for segment b, 0547:59–0847:58 UTC for segment c, and 1132:55–1532:54 UTC for segment d. (U.S. Dept. of State Geographer, ©2011 Europa Technologies, Data SIO, NOAA, U.S. Navy, NGA, GEBCO, ©2011 Google.)

the main objective of the NEAQS experiment was to study air quality, ship tracks were typically designed to trace plume dispersion over the water surface, and as such the ship-track patterns did not display much systematic overlap. A description of experiment goals, preliminary results, and plots of ship tracks can be found online (<http://www.esrl.noaa.gov/csd/ICARTT>).

Below we present time–height cross sections, time series of wind properties, wind profiles showing the different shapes encountered, and distribution histograms for atmospheric heights and layers occupied by a large wind turbine. For convenience, we consider a hypothetical wind turbine whose rotor heights span a 50–150-m vertical layer [similar to the 5-MW turbine with hub height of 102 m and rotor diameter of 116 m described by Käsler et al. (2010)]. The VAD analysis level nearest to the midpoint of this layer is at 95 m, and so “hub height” winds for this “turbine” will be specified for the 95-m

level, even though this is not precisely the midpoint of the “rotor” layer. The examples presented are a sampling of the kinds of analysis that can be performed with the offshore lidar datasets.

3. Wind-flow characteristics

Figure 6 shows time–height cross sections, using data derived from 15-min wind speed profiles plotted along several ship-track segments, off the New England coast in the evening/night (segments a–c) and early morning (segment d) hours of 20–21 July local time (21 July UTC). At sunset (~ 0000 UTC) the ship moved from the coastline of southern Maine toward the open ocean (leg a), then it returned back to the coast (leg b), and then it cruised off the New Hampshire shore toward open ocean again (leg c). During the fourth segment (leg d) the following morning, *RHB* cruised along the coast from Cape

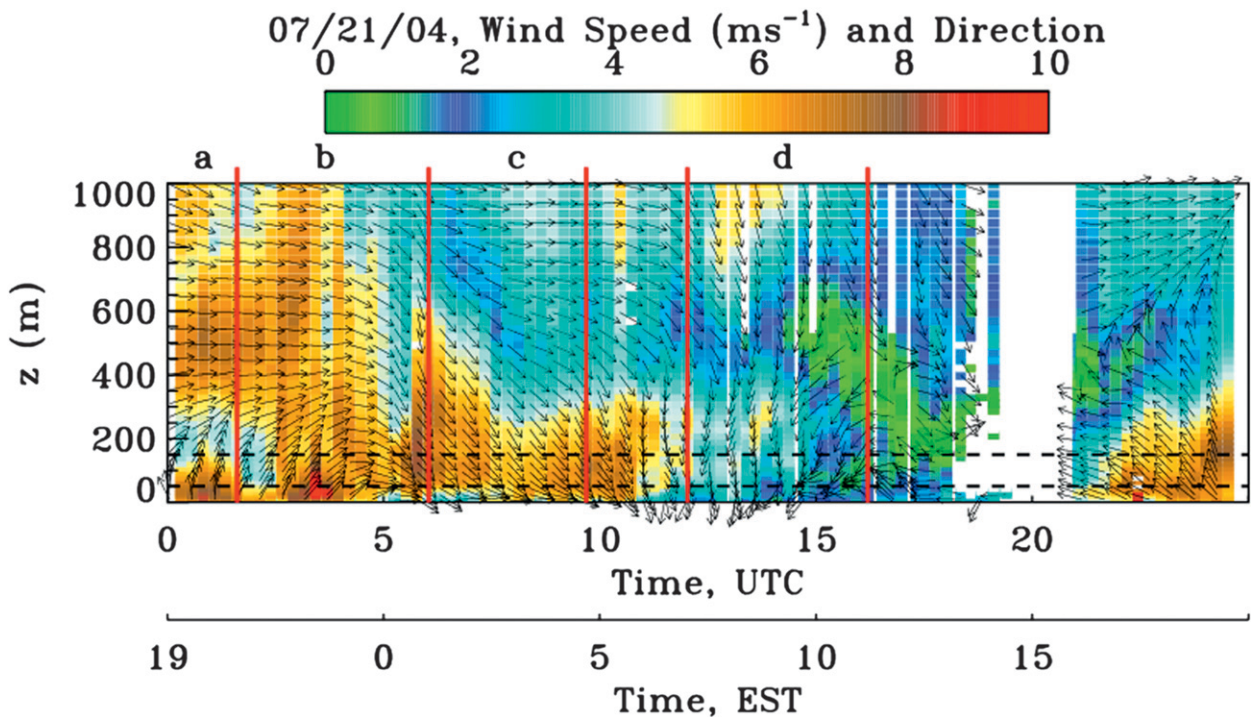


FIG. 7. Mean wind speed [color bar, scaled from 0 (green) to 10 (red) m s^{-1}] and direction (arrows), computed from HRDL conical scans during 21 Jul 2004. Segments a–d are the same as in Fig. 6. Two horizontal dashed lines indicate the hypothetical turbine-rotor-layer height of 50–150 m. The vertical axis is height above sea level (m), and the horizontal axis is time (UTC; local eastern standard time lags UTC by 5 h—see bottom scale), and the color scale at the top is in meters per second. The gap between 1800 and 2000 UTC was due to fog.

Anne to Boston, Massachusetts. These 1.5-km-deep curtains of color-coded wind speeds (see Fig. 7, described below, for color bar) illustrate the strong vertical, horizontal, and temporal variability of the winds aloft often encountered in the coastal zone. Early in the cross section during legs a and b, nocturnal winds of $\sim 6\text{--}7 \text{ m s}^{-1}$ were observed over the entire 1000-m layer, dropping to a 300-m-deep layer in leg c. The wind direction shifted from westerly (leg a) and southwesterly (leg b) to northwesterly (leg c). During next-morning hours (segment d), weak winds of $1\text{--}3 \text{ m s}^{-1}$ blew primarily from northerly directions.

a. 24-h period of observations

A closer look at the wind variability in Fig. 6 is illustrated as a time–height cross section in Fig. 7, where red vertical lines delimit the ship-track segments shown in Fig. 6. Arrows in Fig. 7 indicate wind direction, and the color indicates wind speed magnitude from 0 (green) to 10 (red) m s^{-1} .

Figure 7 shows considerable difference between nighttime (0000–1200 UTC) and daytime ($\sim 1200\text{--}2300$ UTC) winds. At turbine heights of 50–150 m, about 7 h of gently varying winds of $6\text{--}7 \text{ m s}^{-1}$ were observed from 0300 to 1000 UTC, then dropping to $3\text{--}4 \text{ m s}^{-1}$. Later in the

morning, the wind direction changed from northeasterly to easterly (~ 1400 UTC) and became even weaker ($\sim 1 \text{ m s}^{-1}$). An unusual weak-flow feature was observed aloft at this time but was not mimicked at the surface. LLJs, appearing as horizontal bands of higher wind speeds than those above and below, are evident at times from 0000 to 1100 and from 2100 to 0000 UTC. A smooth transition in wind speed and direction between segments in Fig. 7 confirms the success of the motion-compensation procedures in transferring the lidar beam coordinates from the ship frame to the world frame, allowing HRDL to measure and produce consistent real-time winds from the water surface up to several hundred meters.

The time–height cross section in Fig. 7 consists of a succession of vertical color strips each covering a 15-min averaging period and each representing a mean profile of wind speed or wind direction (arrows) from 10 to 1000 m above the surface for that 15-min period. For a more detailed, more quantitative view of the vertical structure, the individual 15-min profiles can be plotted. Examples of such profiles are shown in Fig. 8 up to 500 m to demonstrate details of the most commonly observed conditions on 21 July. Blue profiles in Fig. 8 (left panel) depict almost constant wind speed in the

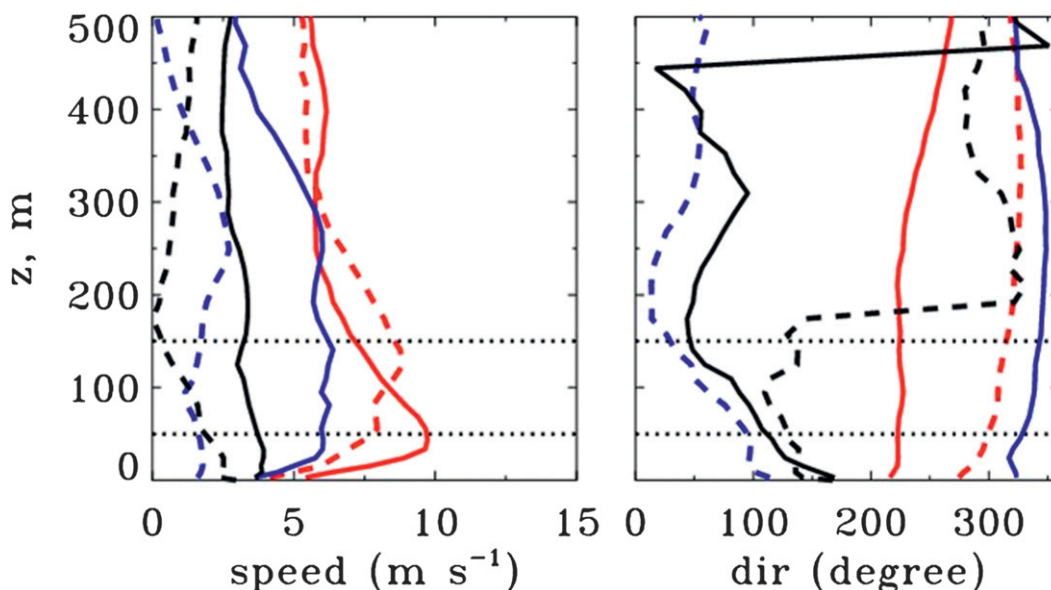


FIG. 8. Examples of wind (left) speed and (right) direction profiles during most observed wind flow situations as described in the text. As in Fig. 7, two horizontal dotted lines indicate the hypothetical turbine-rotor height of 50–150 m. The solid blue lines are 1015 UTC, the dashed blue lines are 1430 UTC, the solid red lines are 0315 UTC, the dashed red lines are 0515 UTC, the solid black lines are 1630 UTC, and the dashed black lines are 1530 UTC.

vertical direction across the turbine-rotor layer, as the direction (right panel) increased slightly (solid line) or decreased linearly (dashed line). Red lines show LLJ-shaped wind profiles with wind speed maxima at the bottom (solid line) or at the top (dashed line) of the

rotor layer; the wind direction was constant or slightly increasing in this layer. Black dashed profiles show a weak-wind period in which the winds decreased with height to almost 0 m s^{-1} at 180 m and there was an $\sim 200^\circ$ shift in wind direction at this height. Black solid

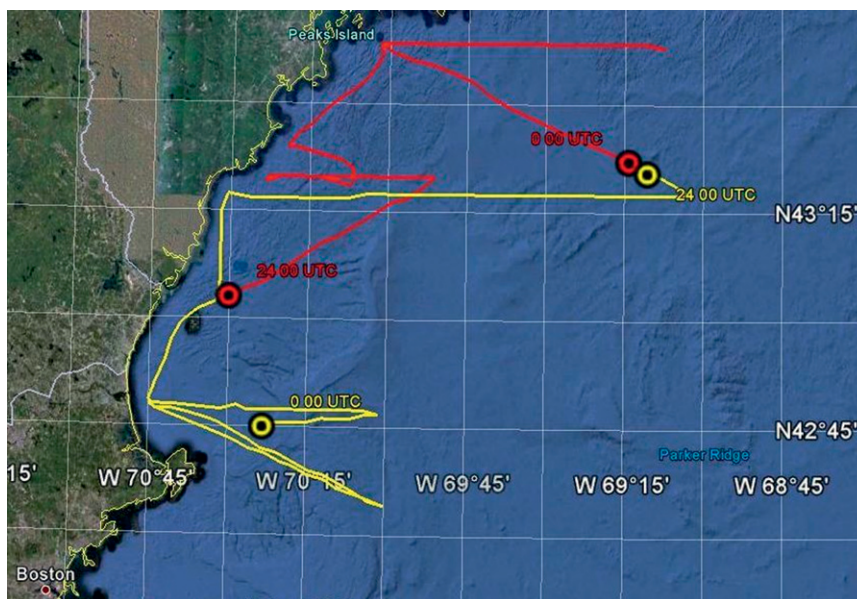


FIG. 9. Ship tracks on 30 (yellow lines) and 31 (red lines) Jul. Disks of the corresponding color indicate the start and the end of the ship track for each day. Longitude/latitude grid is shown with approximate cell dimensions $\Delta x = 20.3 \text{ km}$ and $\Delta y = 27.6 \text{ km}$. (U.S. Dept. of State Geographer, ©2011 Europa Technologies, Data SIO, NOAA, U.S. Navy, NGA, GEBCO, ©2011 Google.)

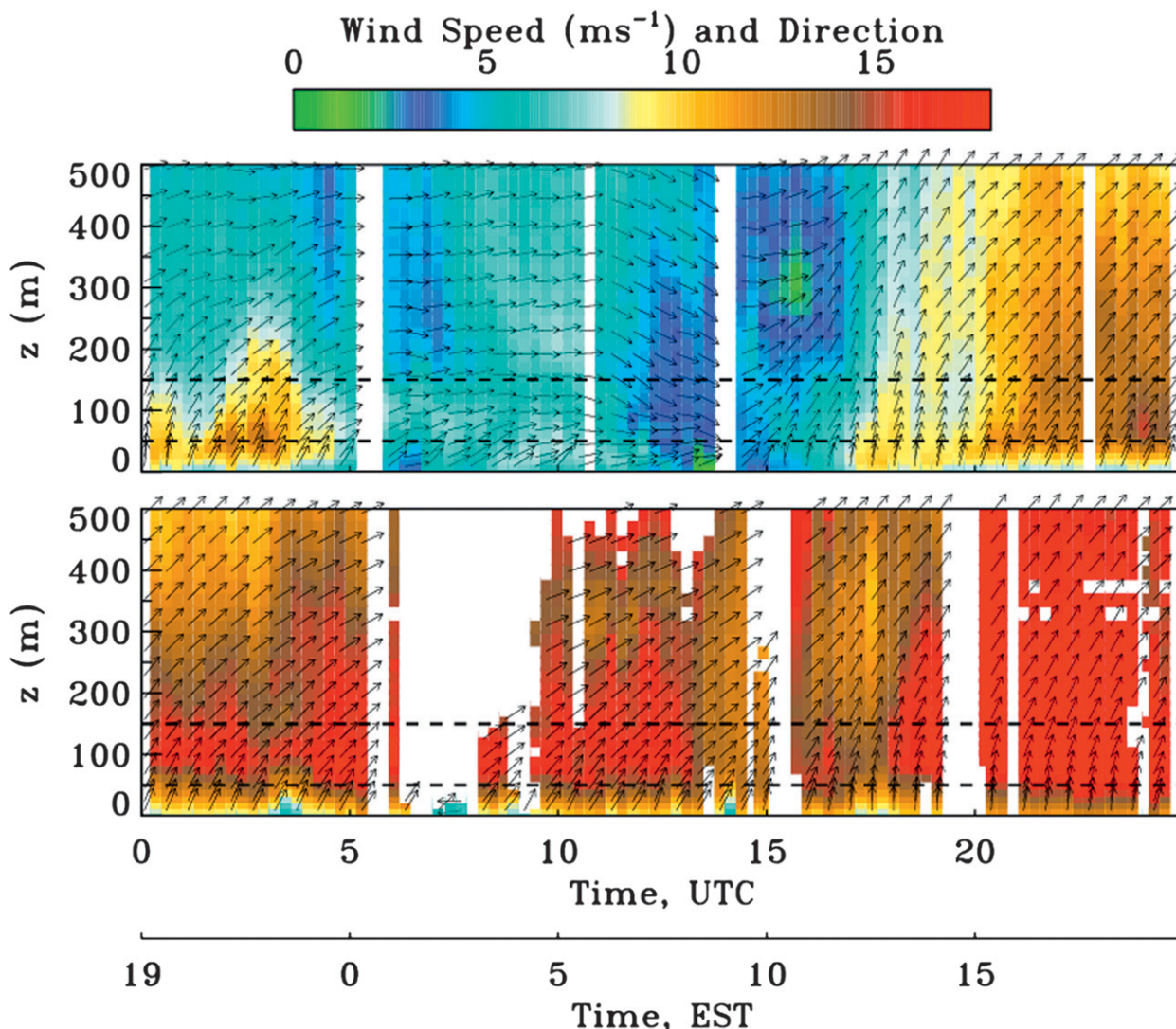


FIG. 10. Time-height cross sections of wind speed computed from HRDL conical scans during (top) 30 and (bottom) 31 Jul 2004. The mean wind speed is indicated by the color bar, scaled from 0 (green) to 18 (red) m s^{-1} , and the direction is shown by arrows. The two horizontal dashed lines indicate a hypothetical turbine rotor height of 50–150 m. The axes are as in Fig. 7. The brief gaps are periods during which scans other than conical scans were being performed, and so further analysis of the dataset would be able to fill in these gaps. The large gap between 0600 and 0800 was during a period of thick marine fog.

profiles illustrate a return to almost constant wind speed and a strong decrease in wind direction through the turbine-blade layer. The magnitude and shape of the wind profiles varied significantly over this 24-h period. This kind of accurate, high-resolution profile data is needed to address many WE requirements.

b. Consecutive days, contrasting wind patterns

Figure 9 shows ship tracks during a 48-h period, where ship movements on 30 and 31 July are shown by yellow and red lines, respectively. On 30 July, the ship cruised in the southern part of the Gulf of Maine, and then it moved north on 31 July. These two consecutive diurnal

periods illustrate the forecasting challenge posed by the strong variability in wind-flow conditions that is often seen from day to day off the New England coast.

Flow conditions in the first 500 m above the water surface are shown Fig. 10, where wind speeds were more than 5 m s^{-1} stronger on 31 July (bottom panel) than on 30 July (top panel). Arrows in both panels in Fig. 10 indicate predominant westerly wind-flow directions becoming southwesterly, but being more variable on 30 July, especially between 1200 and 1800 UTC. Detailed analysis of synoptic conditions is beyond the scope of this paper, but we note that the stronger winds of 31 July, observed in open waters, have been attributed to the

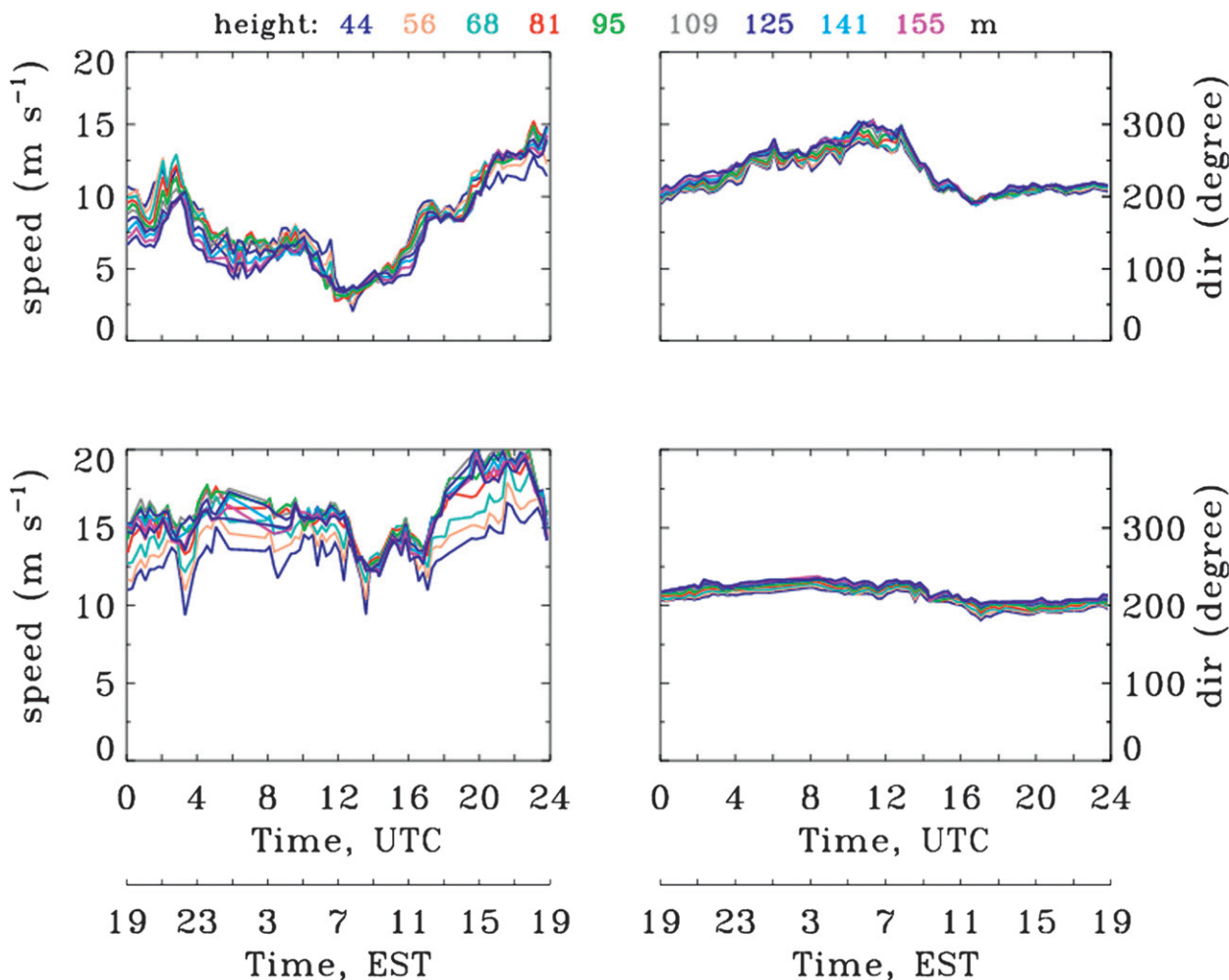


FIG. 11. Time series of (left) wind speed (m s^{-1}) and (right) wind direction ($^{\circ}$ clockwise from north) at several heights (as indicated at the top of the figure) within the turbine-rotor-swept layer for (top) 30 and (bottom) 31 Jul 2004.

approach of the first hurricane of the season, Hurricane Alex, that formed on 31 July and dissipated on 6 August, reaching peak wind speeds of 120 mi h^{-1} (54 m s^{-1}) while off the coast of New England (see online at <http://disc.sci.gsfc.nasa.gov/hurricane/additional/science-focus/HurricaneAlex2004.shtml>).

Low-level jets, an additional source of wind power and the major source of shear-generated turbulence in nighttime hours over flat terrain (e.g., Mahrt 1999; Banta et al. 2002, 2006), were observed much of the time on 31 July, especially prior to 1900 UTC, with wind speed maxima up to 20 m s^{-1} , as compared with only two episodes of weak jet evolution during the nighttime hours (0000–0300 UTC) and evening transitional period (2000–0000 UTC) on 30 July. LLJ structure was evident in the wind profiles during many observational periods of this experiment, often during nighttime and transitional periods, but also during the day on occasion. Thus, similar to

the observation of nocturnal wind profiles in the Great Plains, marine wind profiles often demonstrated occurrences of LLJ structure in the vertical profiles of wind speed (Smedman et al. 1993, 1997; Colle and Novak 2010).

Time series of wind speeds (Fig. 11, left panels) and direction (right panels) at several heights within the turbine-rotor layer show temporal variation in finer detail. On 30 July (top panels), winds at all heights show significant diurnal variation, decreasing to $<5 \text{ m s}^{-1}$ by 1200 UTC (just after sunrise) and increasing again to $>10 \text{ m s}^{-1}$ during the following daytime. A broad span of wind speeds from 2.5 to 13 m s^{-1} was observed during both periods, with values of 7.7 m s^{-1} at night and 8.9 m s^{-1} in the daytime averaged over the hypothetical turbine-rotor layer (50–150 m). The time series show significant changes of sometimes several meters per second occurring over time periods as short as 30 min (e.g., at 0300 and 1600 UTC).

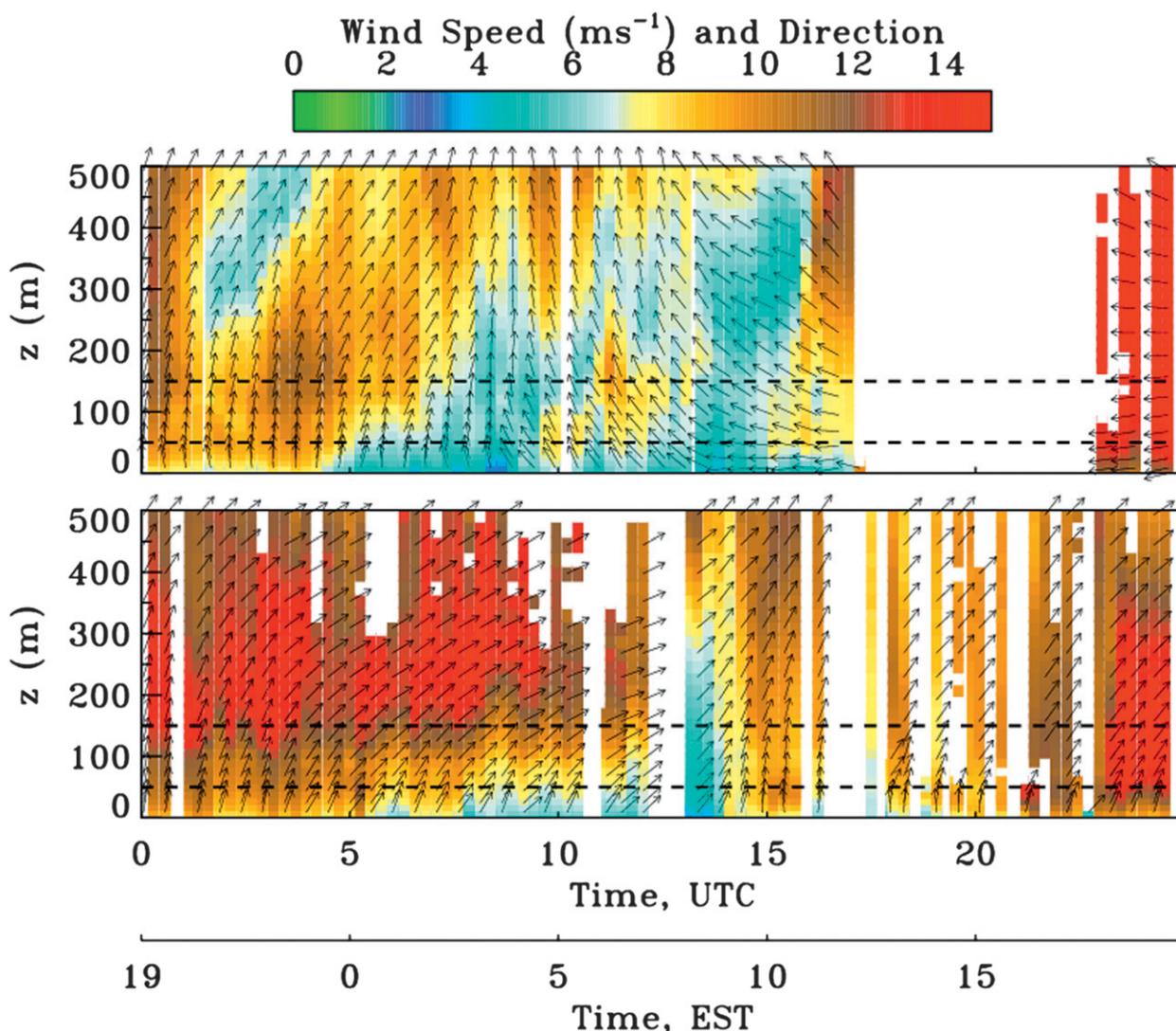


FIG. 12. Time–height cross section of mean wind speed and direction, obtained from lidar conical scans performed at fixed shallow (2° – 16°) elevation angles during the 12-h periods of (top) 13 and (bottom) 16 Jul 2004, when *RHB* was stationed in Boston Harbor. Axes are as in Fig. 7; color scale goes up to 15 m s^{-1} . The data gap between 1700 and 2200 UTC in the top panel is for a period of steady rain, and gaps above 300 m were for a broken stratocumulus deck. Gaps shown in the bottom panel between 1200 and 2200 were when scans other than conical cans were being performed.

On 31 July, the rotor-layer mean-wind speeds were strongest for the entire period of HRDL measurements for this cruise, ranging from 10 to 20 m s^{-1} , with a mean nighttime value of 14 m s^{-1} and daytime value of 15 m s^{-1} . The corresponding mean wind directions in this layer were 232° and 214° . Stronger diurnal variation in wind direction was observed for the lighter winds on 30 July, with mean direction of 242° at night and 216° during daytime. Stronger vertical shear of the horizontal wind speed, indicated by the separations between the wind traces at the different levels, was also evident on 31 July.

Besides the differences in meteorological conditions between the two days, the differences in wind properties

also reflect spatial differences in the location of the ship tracks, leading to the measurements being taken at different offshore distances or locations along the coastline. In the next two sections we isolate instances of temporal and spatial variability found in wind flows in the coastal zone.

c. Measurements from a stationary position

Figure 12 shows two examples of fixed-location measurements, when *RHB* was stationed in Boston Harbor during nighttime hours (0000–1200 UTC) on 13 and 16 July. Concurrent air-chemistry measurements (not shown) indicate that the night of 13 July was characterized by

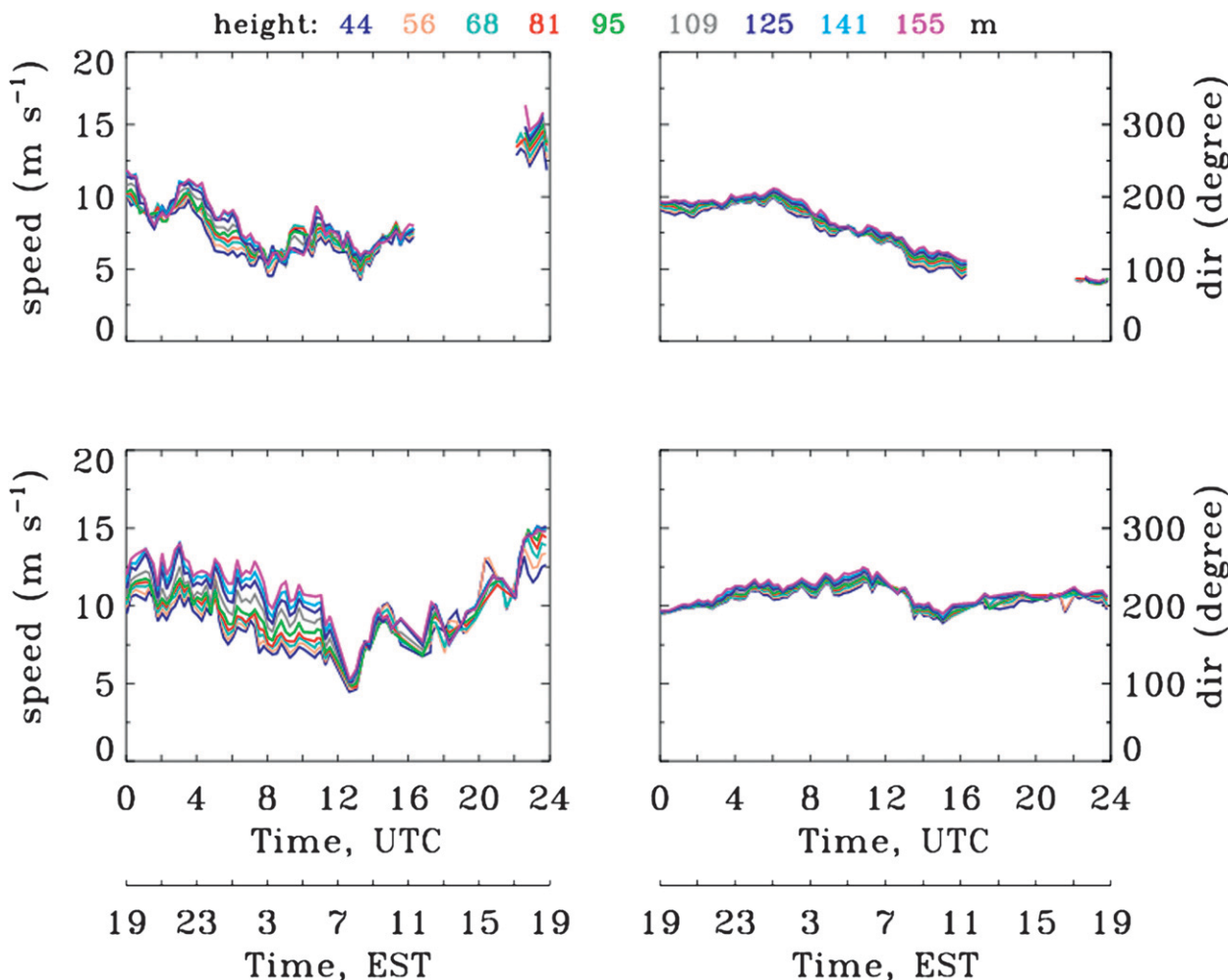


FIG. 13. Time series of 15-min-averaged (left) wind speed and (right) wind direction measured by HRDL at several heights across the turbine-rotor-swept area are shown for (top) 13 and (bottom) 16 Jul 2004.

transitional flow shifting from polluted continental to clean oceanic air: south-southwesterly winds shifted to southerly at ~0700 UTC and then to almost easterly during the morning transitional period (at ~1200 UTC). LLJs were observed during the period of 0200–0500 UTC, with wind speed maxima reaching 10–11 m s⁻¹ at 160–180 m. During the night of 16 July, LLJ winds with sustained west-southwesterly flow were several meters per second stronger than those on the night of 13 July. LLJs having distinct maxima in the vertical direction were observed in 71% of 15-min profiles throughout the night, from 0000 to 1000 UTC. The rest of the profiles showed more complex, layered structure [type-III profiles, as in Pichugina and Banta (2010)] with strong shear in the lowest 200 m.

Vertical differences in wind speed (shear) can be seen in time series of wind characteristics at different heights, as shown in Fig. 13. Such vertical information can be

used to provide an accurate estimate of winds across the rotor layer, which can be used to provide distributions and statistics of the calculated quantities, as shown in histograms of the distributions of mean wind speed, direction, and shear averaged across the rotor layer in Fig. 14 for the nocturnal LLJ period. It will be shown in the next section that for the entire project period winds were stronger at night, presumably largely because of the LLJ activity seen in the time–height cross sections. This plot shows that wind speeds in the rotor layer can vary over a wide range of values, even on individual nights. As expected, shear magnitudes were larger on the stronger-wind day.

d. Spatial variability

Cross sections such as Figs. 6, 7, and 10 show considerable variability in wind speed and direction along the ship track. Some of this variability may result from spatial

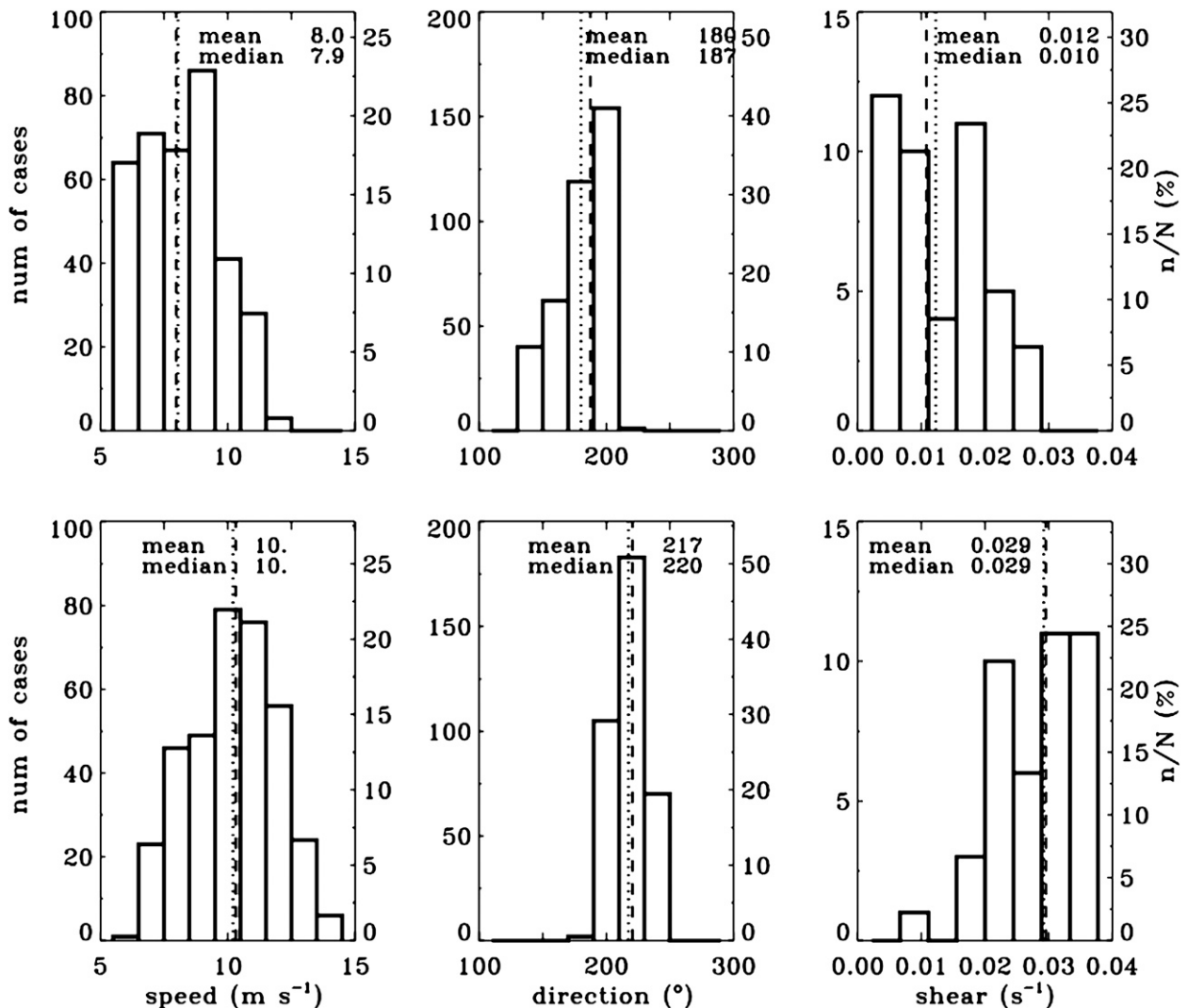


FIG. 14. Nighttime distribution of wind (left) speed, (center) direction, and (right) shear averaged over the 50–150-m rotor layer on (top) 13 and (bottom) 16 Jul, as calculated from HRDL profile data. Dotted lines in all plots indicate means, and dashed lines represent the medians of the sample.

variability of the flow field, but some is due to the evolution of the wind field, as shown in the previous section. In other words, the variations in the winds in Figs. 6, 7, and 10 are a combination of true spatial variability and temporal changes affecting the entire region—such cross sections do not unequivocally demonstrate spatial variability.

Isolated in situ or profiling instrumentation on a fixed mast or platform is incapable of detecting horizontal variability, and so the representativeness of such measurements is an issue. *Arrays* of fixed measurements can sample horizontal variability, but the relevant spatial scales of variability must be known and factored into the array design. Scanning remote sensing instrumentation can be used to determine scales that are smaller than the scan diameter.

The other way to sample spatial variability is by using mobile platforms, such as the ship *RHB*. Unequivocal identification of spatial changes is possible by retracing the ship path back and forth over an area. Although such patterns were not performed often during NEAQS, the bottom-left panel of Fig. 15 shows one example in which the *RHB* retraced the same course three times on 11 August. These legs are marked a, b, and c on the time–height cross section for this day (Fig. 15, top panel). Replotted as longitude plots in the bottom-right panels of Fig. 15 with west to the left, these legs show persistence of the spatial patterns in time. This repeatability indicates genuine spatial patterns in the wind features, such as the LLJ at 300-m height on the east side of the cross sections, which is especially evident in legs b and c.

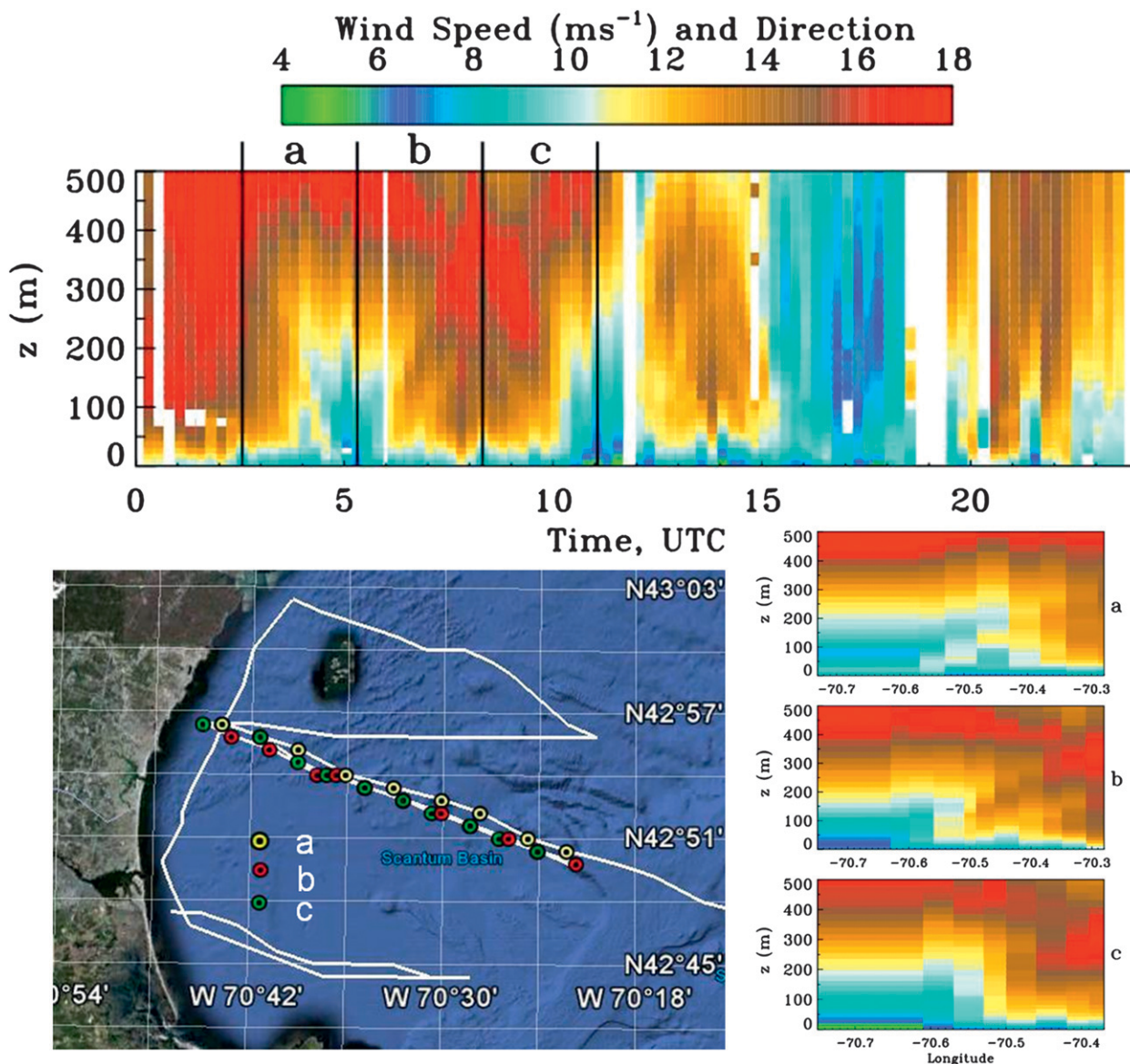


FIG. 15. (top) Time–height cross section of mean wind speed, computed from HRDL conical scans during 11 Aug 2004 [axes as in Fig. 7; the color bar is scaled from 4 (green) to 18 (red) m s^{-1}]. Black vertical lines in the top panel indicate three segments shown by circles on the (bottom left) ship track. Brief gaps in the top plot show periods during which scans other than conical scans were being performed. (bottom right) Plots of mean wind speeds for these segments as a function of longitude. (U.S. Dept. of State Geographer, ©2011 Europa Technologies, Data SIO, NOAA, U.S. Navy, NGA, GEBCO, ©2011 Google.)

A research vessel is a slow-moving mobile platform, and therefore flow features can evolve during transit times of several hours. Airborne platforms can sample the spatial variability more directly. A dramatic example is the airborne Doppler lidar measurements reported by Rothermel et al. (1998), which showed strong horizontal and vertical structure in the lowest few hundred meters of the marine airflow past Point Arena, California. A potential effective companion to shipborne Doppler lidar would be an instrumented unattended airborne vehicle,

which could sample the horizontal flow variability at a vertical level of interest while the lidar documented the flow-field evolution through a deeper layer.

4. Campaign statistics

Statistics and distributions can also be calculated for longer time periods than the daily statistics presented in section 3c. In this section, we present statistics for the duration of the project calculated from all available

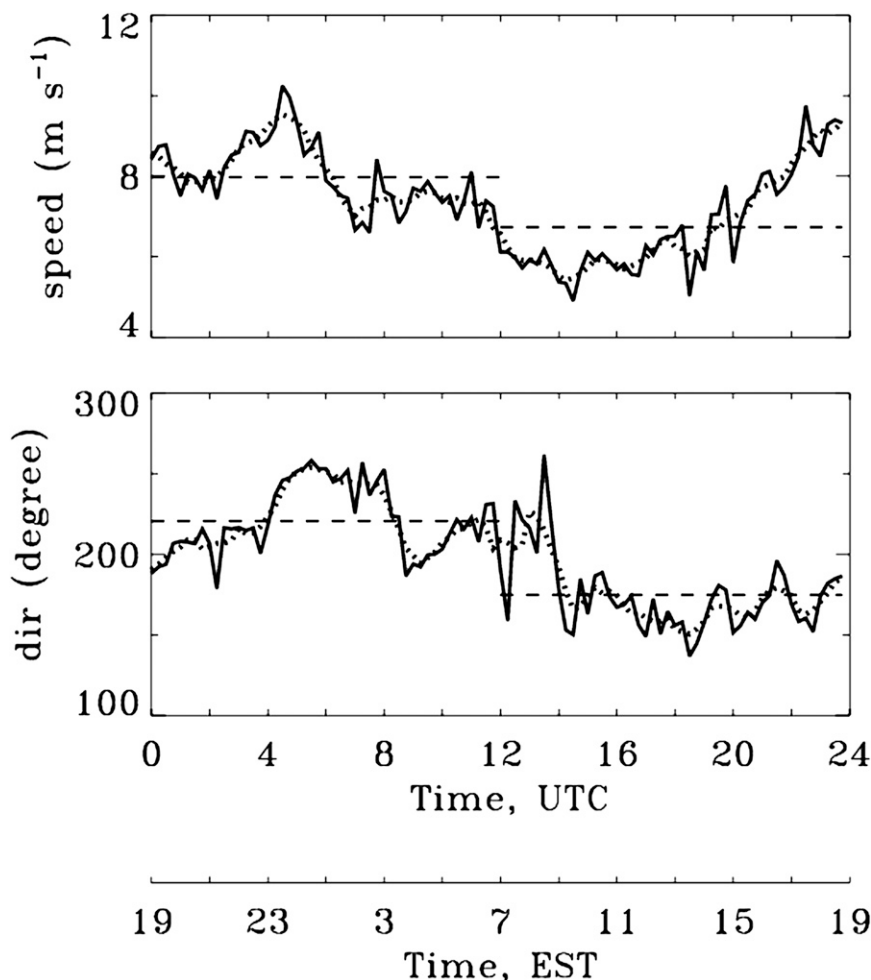


FIG. 16. Time series of mean wind speed and direction at 95 m above the water surface for the entire campaign. Solid lines are 15-min averaged data; dotted lines are 1-h averaged data. Dashed lines are nighttime (0000–1200 UTC) and daytime (1200–0000 UTC next day) means.

Doppler lidar profiles for mean wind speed and shear across the blade layer, as examples of longer-term averages. Because few if any other long-term measurements are available aloft in the blade layer over the ocean, these measurements could be considered to be a first guess for a summertime climatological description of winds aloft in this layer over the Gulf of Maine. Longer-term deployments would be needed to calculate annual averages.

Examples of monthly mean 95-m wind data for the diurnal cycle are presented in Fig. 16 at 15-min (solid lines) and hourly (dotted lines) intervals of the daily cycle. Summer is the lowest wind-resource season, although the average wind speeds shown here are still greater than 7 m s^{-1} . The strongest winds of $\sim 10 \text{ m s}^{-1}$ were observed at 0400–0500 UTC, when the wind blew

on average from the southwest (240°), and the weakest winds of just greater than 5 m s^{-1} were observed during morning hours (1200–1800 UTC) in mean south-southeasterly flow. An interesting aspect is the steady increase in the hourly wind speeds evident through the afternoon hours starting at 1800 UTC and peaking after 2300 UTC at about sunset. Overall, nighttime southerly winds at 95 m above the water surface were $1\text{--}2 \text{ m s}^{-1}$ stronger than the southeasterly daytime winds.

a. Wind speed and shear

The distributions of wind speed over the 50–150-m rotor layer for the entire project period are shown in Fig. 17 (top panels). Means and medians of distributions are shown in both panels by solid and dotted lines, respectively. The nighttime distribution is broad, $6\text{--}12 \text{ m s}^{-1}$,

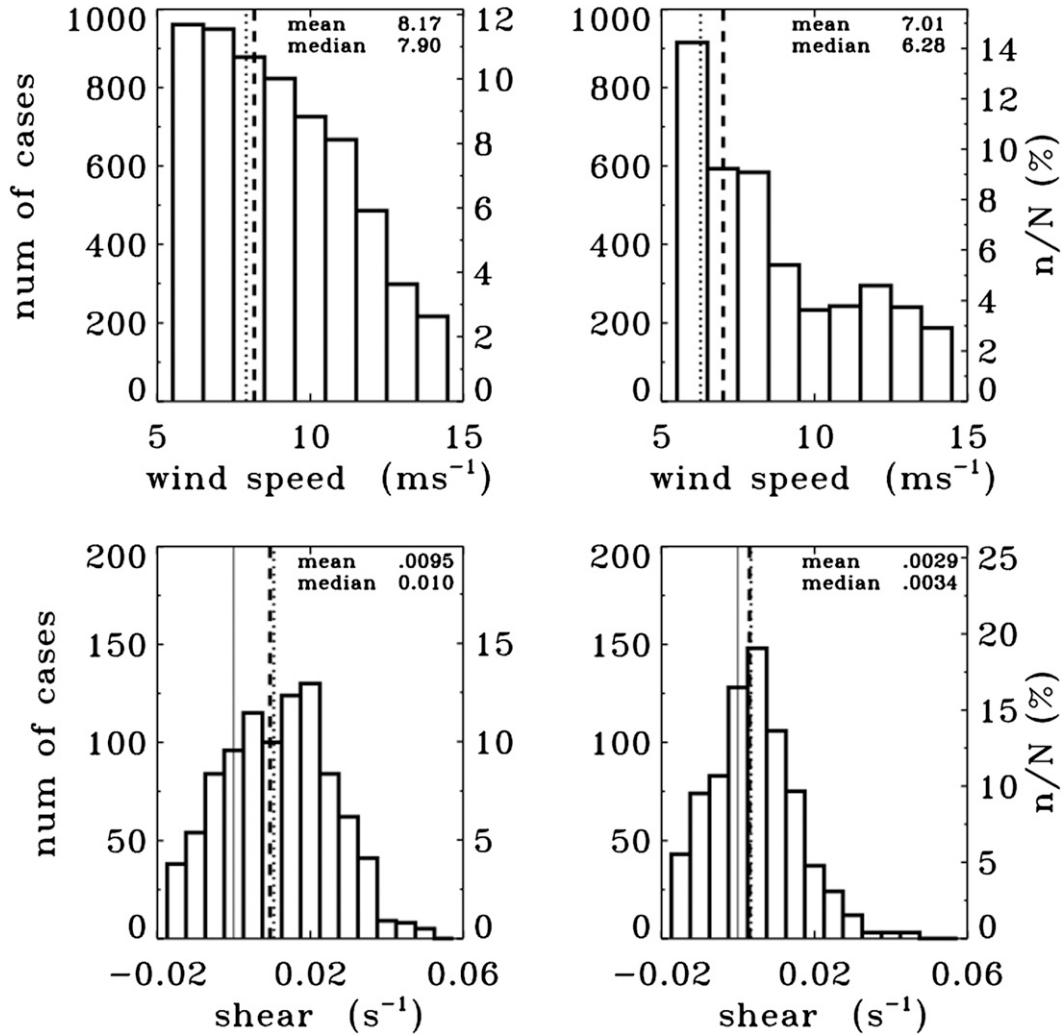


FIG. 17. Distribution of mean wind (top) speed and (bottom) shear across the 50–150-m layer for the (left) nighttime and (right) daytime hours during NEAQS. Mean values of the each distribution are shown by dashed lines, and medians are shown by dotted lines. Solid lines in the bottom plots indicate zero; note that negative shear values, where wind speed decreases with height, were found.

whereas the daytime winds are mostly less than 9 m s^{-1} , although a weak secondary maximum of 13 m s^{-1} may reflect the late-afternoon increases in wind speed.

Vertical shear of the horizontal wind is another important quantity. Profiles of high precision and high temporal and vertical resolutions, as provided by HRDL, are essential for accurately estimating speed and directional shear of the wind at turbine-rotor heights. Distributions of wind shear across the 50–150-m layer of the atmosphere for the nighttime (0000–1200 UTC; left panel) and daytime (1200–0000 UTC next day; right panel) hours are also shown in Fig. 17 (bottom panels). Both histograms show larger mean and median values at night, but with a similar range of the observed wind shear values for nighttime and daytime, reaching peak values

of 0.05 s^{-1} at night. It has been shown (Pichugina et al. 2010) that steadier offshore winds resulted in monthly-averaged nighttime wind shear values across the rotor heights (50–150 m) that are similar to those shown here but that are one-half as large (0.021 s^{-1}) as nighttime observations over flat terrain near Lamar, Colorado (0.048 s^{-1}), or in Kansas (0.039 s^{-1}), where the shear was often found to be constant with height in the stable boundary layer. Note that larger shears of 0.10 s^{-1} have been routinely measured in the layer below the LLJ nose over land (Banta et al. 2003; Sun et al. 2012).

b. Power-law wind profiles

The assumption of a power-law wind-profile relation, $U = U_{\text{ref}}(z/z_{\text{ref}})^\alpha$, is a common approach used to

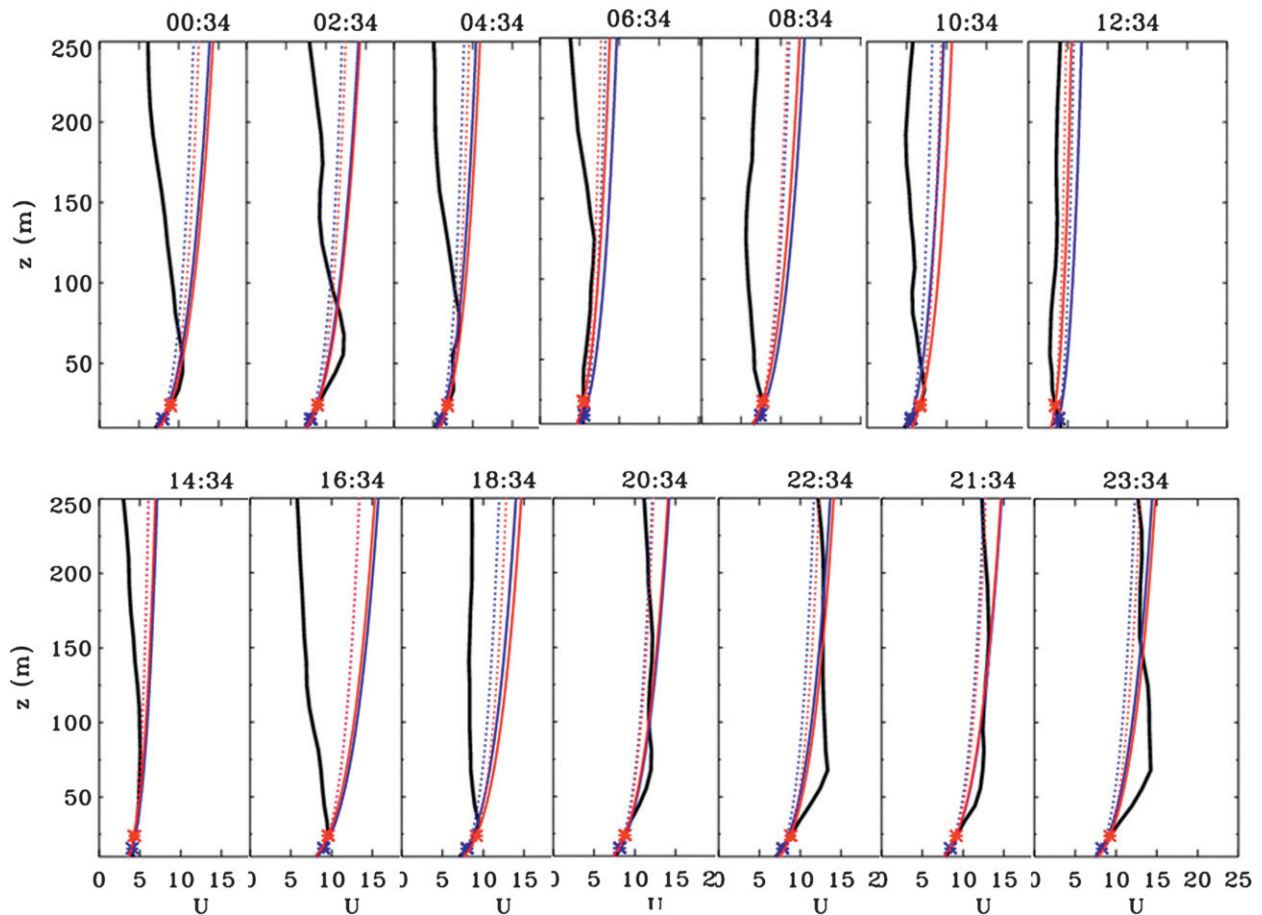


FIG. 18. Examples of HRDL-measured wind profiles during 30 Jul 2004 are shown by thick black lines. Color lines represent normal wind profiles computed with two different shear exponents (dotted indicates computed with $\alpha = 1/7$, and solid is for $\alpha = 0.2$), and base reference-level wind speed measured at two different heights (blue asterisk indicates measured at $z = 15$ m, red asterisk is for $z = 25$ m).

estimate the wind speed U at a higher elevation z using near-surface, tower measurements (often at 5–15 m, but occasionally up to 40 m) of wind speed U_{ref} at a height z_{ref} on the tower. The “shear exponent” α , specified by the International Electrotechnical Commission for power-law or “normal” wind profiles for a turbine-rated wind speed near 12 m s^{-1} and a hub height of 80–90 m as routinely used in WE, is often taken to be either $1/7$ or 0.2 .

Illustrative examples of deviations of measured wind profiles from those computed by power law, using combinations of the two values of the shear exponent and wind speed at two reference heights, are given in Fig. 18 for the night of 30 July. HRDL-measured wind profiles in Fig. 18 are shown by thick solid black lines. Normal wind profiles computed with two base velocities U_{ref} at 15 and 25 m are shown by blue and red lines, respectively, where solid lines represent profiles computed with an exponent of 0.2 and dotted lines are computed with an exponent of

$1/7$. Strong deviations from the measured values are often evident in the calculated profiles. Thus, it appears that the use of measured profiles should be preferred for WE applications, where high precision is important.

These 15-min profiles were arbitrarily chosen for every second hour during nighttime (Fig. 18, top panel) and daytime (Fig. 18, bottom panel) periods on 30 July. They are not carefully selected profiles to show worst cases. This night, as shown in Fig. 10, was a relatively quiet night with moderate wind speeds, small wind and directional shear across the rotor height, and a clear diurnal pattern in wind speed and direction (Fig. 11). The below-rated speed values illustrated here are in the ascending branch of the power curves (wind speed vs power output) for most turbines, where the power output is most sensitive to wind speed.

From analysis of 15-min profiles from the experiment, we can conclude that occasional individual profiles may show reasonable agreement (within $\sim 20\text{--}30 \text{ cm s}^{-1}$) up to

60–80 m (see sample profiles at 0034 and 1434 UTC), and sometimes even higher—up to 100 m (0434 UTC). Most of the profiles in the entire dataset, however, show significant departures of several meters per second from the power-law profiles—and, in fact, show little resemblance to any standard profiles, including logarithmic and diabatic, in the 50–150-m layer. The strongest deviations between computed and measured wind speed profiles, which reached 7.7 m s^{-1} , were observed for strong wind speeds ($>10 \text{ m s}^{-1}$) and LLJ-shaped profiles, which often have a near-linear shape to the profile below the LLJ maximum (Banta et al. 2003, 2006), in contrast with the power-law wind-profile shape. These results are also in good agreement with results of inland HRDL measurements in the flat terrain of the Great Plains, where significant deviations from logarithmic or power-law profiles were found in the lowest few hundred meters for stable conditions—frequently in the presence of strong low-level jets.

5. Conclusions

Despite the relatively smooth, flat surface of the ocean (as compared with land surfaces), the measurements presented here indicate strong spatial and temporal variability of the wind field in the offshore region, in the atmospheric layer aloft occupied by turbine rotors, and demonstrate the need for better and more extensive observations in the layer. Much of what is currently believed to be known about this offshore layer is inferred from numerical or conceptual models or is inferred from data obtained near the ocean surface or obtained on land along the coast. Instances are rare in which information from these sources has been verified against actual high-quality data aloft in this layer, because measurements in this layer themselves are rare. In this paper we have shown the potential for obtaining and using such high-quality measured data to address the wide spectrum of U.S. offshore wind-energy needs.

Accurate, high-resolution measured profile data, when available, are generally superior to those produced by models or surface observations in determining quantities of interest to WE. For example, Pichugina et al. (2010) have shown that such profiles provide accurate estimates of stable boundary layer depth, a traditionally difficult measurement, and Tucker et al. (2009) showed that shipboard lidar-measured turbulence profiles can be used to provide boundary layer depth measurements over the ocean 24 h per day. Profile data are also important for assessing errors associated with using standardized (e.g., power law) profiles to extrapolate wind speed values from near the surface to turbine hub height, to find alternative approaches, and for characterizing the speed and directional shear across the blade layer. Examples of

such measurements using a Doppler lidar have been presented in this paper. The lidar observations also show that near-surface winds often do not “see” many of the changes in the flow aloft, some of which were significant. Thus, near-surface measurements, or even low-resolution profile measurements, often produce misleading results when extrapolated to hub height. Such results can lead to significant error in estimates of turbine power output.

Lidar datasets extending over multiweek periods, such as NEAQS and the others listed in Table 1, allow some generalizations to be made about the turbine environment. Diurnal cycles in wind speed were seen to occur on most days. A high frequency of LLJs was evident, especially at night during the project, and as a result wind speeds in the rotor layer on average were found to be stronger at night. Therefore, as over land, it is important to determine how well NWP models are doing in estimating the structure and dynamics of LLJs in this region.

An important issue for WE is horizontal variability, the existence of persistent regions of higher mean wind speeds that may be associated with coastal irregularities or onshore topography. Such regions would be favored for energy generation, whereas other regions of reduced winds may not be, and so it is obviously important to be able to identify the more favorable locations. Horizontal variability also impacts the preferred techniques for *sampling* the flow field, however. The design of offshore arrays of measurements aloft must be able to sample this variability. Because factors such as typical distance scales are currently unknown, it is also unknown whether NWP models are characterizing this variability properly. Mobile platforms such as ships equipped with high-resolution profiling instrumentation provide an important capability for investigating these types of variability, as illustrated in this study.

Scanning, pulsed Doppler lidar instruments operated from fixed platforms or ships (equipped with effective motion compensation) are well suited for providing much improved characterization of offshore wind fields for use in evaluating potential WE sites. By combining scan sequences, including both conical scans at multiple elevation angles and vertical scans at several azimuth angles, high-vertical-resolution horizontal wind field profiles, as well as estimates of turbulence profile, can be routinely obtained several times per hour. Thus, long-term lidar operation at a given site enables compilation of statistics on both the vertical structure and temporal variability of the wind. With the exception of heavily instrumented towers, which are difficult to deploy to heights corresponding to a large turbine, no other measurement technique provides an equivalent site-assessment capability.

The existing datasets of HRDL offshore measurements represent a resource that can be used to understand

better the range of atmospheric conditions, and their spatial and temporal variability, that are encountered by offshore wind turbines above the surface at the level of the rotor blades, to validate numerical models using retrospective runs, to support satellite estimates of wind resources, and to supplement the development of offshore wind-resource maps. This paper has presented a sampling of the kind of information available in these datasets. In addition to the “mining” of existing lidar and other remote sensing datasets to gain greater insight into the characteristics of offshore flows at turbine heights, information from scanning Doppler lidar systems would be a valuable asset in measurement campaigns operated from fixed platforms to address a number of other issues, including

- obtaining wind profiles at a distance from the platform where the flow is not subject to platform-induced distortion effects, using specialized scanning and analysis techniques;
- assessing the flow distortion induced by the platform using scanning mode; and
- providing accurate profiles of the wind to assess the error in measurements from candidate moveable-platform systems deployed to the ocean nearby.

Acknowledgments. We thank our colleagues Sara Tucker, Richard Marchbanks, Janet Machol, Dan Law, Rob K. Newsom, and Brandi McCarty for long hours spent collecting HRDL data on ship. Funding for this project was from the NOAA Air Quality Program, NEAQS, and the Advanced Sensor Application Program (ASAP).

REFERENCES

- Angevine, W. M., J. E. Hare, C. W. Fairall, D. E. Wolfe, R. J. Hill, W. A. Brewer, and A. B. White, 2006: Structure and formation of the highly stable marine boundary layer over the Gulf of Maine. *J. Geophys. Res.*, **111**, D23S22, doi:10.1029/2006JD007465.
- Banakh, V. A., I. N. Smalikho, Y. L. Pichugina, and W. A. Brewer, 2010: Representativeness of measurements of the dissipation rate of turbulence energy by scanning Doppler lidar. *Atmos. Oceanic Opt.*, **23** (1), 48–54.
- Banta, R. M., R. K. Newsom, J. K. Lundquist, Y. L. Pichugina, R. L. Coulter, and L. Mahrt, 2002: Nocturnal low-level jet characteristics over Kansas during CASES-99. *Bound.-Layer Meteor.*, **105**, 221–252.
- , Y. L. Pichugina, and R. K. Newsom, 2003: Relationship between low-level jet properties and turbulence kinetic energy in the nocturnal stable boundary layer. *J. Atmos. Sci.*, **60**, 2549–2555.
- , —, and W. A. Brewer, 2006: Turbulent velocity-variance profiles in the stable boundary layer generated by a nocturnal low-level jet. *J. Atmos. Sci.*, **63**, 2700–2719.
- Browning, K. A., and R. Wexler, 1968: The determination of kinematic properties of a wind field using Doppler radar. *J. Appl. Meteor.*, **7**, 105–113.
- Colle, B. A., and D. R. Novak, 2010: The New York bight jet: Climatology and dynamical evolution. *Mon. Wea. Rev.*, **138**, 2385–2404.
- Darby, L. S., and Coauthors, 2002: Vertical variations in O₃ concentrations before and after a gust front passage. *J. Geophys. Res.*, **107**, 4321, doi:10.1029/2001JD000996.
- , and Coauthors, 2007: Ozone differences between near-coastal and offshore sites in New England: Role of meteorology. *J. Geophys. Res.*, **112**, D16S91, doi:10.1029/2007JD008446.
- Drobinski, P., P. Carlotti, R. K. Newsom, R. M. Banta, R. C. Foster, and J.-L. Redelsperger, 2004: The structure of the near-neutral atmospheric surface layer. *J. Atmos. Sci.*, **61**, 699–714.
- Emeis, S., M. Harris, and R. M. Banta, 2007: Boundary-layer anemometry by optical remote sensing for wind energy applications. *Meteor. Z.*, **16**, 337–347.
- Fairall, C. W., and Coauthors, 2006: Coastal effects on turbulent bulk transfer coefficients and ozone deposition velocity in ICARTT. *J. Geophys. Res.*, **111**, D23S20, doi:10.1029/2006JD007597.
- Grund, C. J., R. M. Banta, J. L. George, J. N. Howell, M. J. Post, R. A. Richter, and A. M. Weickmann, 2001: High-resolution Doppler lidar for boundary layer and cloud research. *J. Atmos. Oceanic Technol.*, **18**, 376–393.
- Hall, F. F., R. M. Huffaker, R. M. Hardesty, M. E. Jackson, T. R. Lawrence, M. J. Post, R. A. Richter, and B. F. Weber, 1984: Wind measurement accuracy of the NOAA pulsed infrared Doppler lidar. *Appl. Opt.*, **23**, 2503–2506.
- Käsler, Y., S. Rahm, R. Simmet, and M. Kuhn, 2010: Wake measurements of a multi-MW wind turbine with coherent long-range pulsed Doppler wind lidar. *J. Atmos. Oceanic Technol.*, **27**, 1529–1532.
- Kelley, N., B. J. Jonkman, G. N. Scott, and Y. L. Pichugina, 2007: Comparing pulsed Doppler LIDAR with SODAR and direct measurements for wind assessment. *WindPower 2007 Conf.*, Los Angeles, CA, American Wind Energy Association, NREL/CP-500-417.
- Kindler, D., A. Oldroyd, A. MacAskill, and D. Finch, 2007: An eight month test campaign of the Qinetiq ZephIR system: Preliminary results. *Meteor. Z.*, **16**, 479–489.
- Lhermitte, R., and D. Atlas, 1961: Precipitation motion by pulse Doppler radar. Preprints, *Ninth Conf. on Radar Meteorology*, Kansas City, MO, Amer. Meteor. Soc., 218–223.
- Lindsay, J., 2010: Cape Wind offshore wind farm gets OK. *Nashua Telegraph*, 29 April 2010.
- Mahrt, L., 1999: Stratified atmospheric boundary layers. *Bound.-Layer Meteor.*, **90**, 375–396.
- Mann, J., A. Peña, F. Bingöl, R. Wagner, and M. S. Courtney, 2010: Lidar scanning of momentum flux in and above the atmospheric surface layer. *J. Atmos. Oceanic Technol.*, **27**, 959–976.
- Musial, W., and S. Butterfield, 2004: Future for offshore wind energy in the United States. Preprints, *Energy Ocean 2004*, Palm Beach, FL, Energy Ocean International (Conf. Paper NREL/CP-500-36313), 16 pp. [Available online at <http://www.nrel.gov/docs/fy04osti/36313.pdf>.]
- , and B. Ram, 2010: Large-scale offshore wind power in the United States: Assessment of opportunities and barriers. NREL Tech. Paper NREL/TP-500-40745, 221 pp. [Available online at <http://www.nrel.gov/wind/pdfs/40745.pdf>.]
- Newsom, R. K., and R. M. Banta, 2003: Shear-flow instability in the stable nocturnal boundary layer as observed by Doppler lidar during CASES-99. *J. Atmos. Sci.*, **60**, 16–33.

- Peña, A., C. B. Hasager, S.-E. Gryning, M. Courtney, I. Antoniou, and T. Mikkelsen, 2008: Measurements and modelling of the wind speed profile in the marine atmospheric boundary layer. *Bound.-Layer Meteor.*, **129**, 479–495.
- , —, —, —, and —, 2009: Offshore wind profiling using light detection and ranging measurements. *Wind Energy*, **12**, 105–124.
- Pichugina, Y. L., and R. M. Banta, 2010: Stable boundary-layer depth from high-resolution measurements of the mean wind profile. *J. Appl. Meteor. Climatol.*, **49**, 20–35.
- , —, W. A. Brewer, B. Jonkman, R. K. Newsom, S. C. Tucker, and W. A. Brewer, 2008: Horizontal-velocity and variance measurements in the stable boundary layer using Doppler lidar: Sensitivity to averaging procedures. *J. Atmos. Oceanic Technol.*, **25**, 1307–1327.
- , —, —, R. M. Hardesty, and C. J. Senff, 2010: Doppler lidar measurements of wind flow characteristics over flat terrain and over ocean. *Int. Symp. for the Advancement of Boundary Layer Remote Sensing*, Paris, France, International Society of Acoustic Remote Sensing of the Atmosphere and Oceans, O-Win-03.
- Rothermel, J., and Coauthors, 1998: The Multi-Center Airborne Coherent Atmospheric Wind Sensor. *Bull. Amer. Meteor. Soc.*, **79**, 581–599.
- Schreck, S., J. K. Lundquist, and W. Shaw, 2008: Research needs for wind resource characterization. NREL Rep. TP-500-43521, 116 pp.
- Smedman, A.-S., M. Tjernström, and U. Högström, 1993: Analysis of the turbulence structure of a marine low-level jet. *Bound.-Layer Meteor.*, **66**, 105–126.
- , H. Bergström, and B. Grisogano, 1997: Evolution of stable internal boundary layers over a cold sea. *J. Geophys. Res.*, **102**, 1091–1099.
- Smith, D. A., M. Harris, A. S. Coffey, T. Mikkelsen, H. E. Jørgensen, J. Mann, and R. Danielian, 2006: Wind lidar evaluation at the Danish wind test site in Høvsøre. *Wind Energy*, **9**, 87–93.
- Sun, J., L. Mahrt, R. M. Banta, and Y. L. Pichugina, 2012: Turbulence regimes and turbulence intermittency in the stable boundary layer during CASES99. *J. Atmos. Sci.*, **69**, 338–351.
- Tucker, S. C., W. A. Brewer, R. M. Banta, C. J. Senff, S. P. Sandberg, D. Law, A. M. Weickmann, and R. M. Hardesty, 2009: Doppler lidar estimation of mixing height using turbulence, shear, and aerosol profiles. *J. Atmos. Oceanic Technol.*, **26**, 673–688.
- , and Coauthors, 2010: Relationships of coastal nocturnal boundary layer winds and turbulence to Houston ozone concentrations during TexAQS 2006. *J. Geophys. Res.*, **115**, D10304, doi:10.1029/2009JD013169.
- White, A. B., and Coauthors, 2007: Comparing the impact of meteorological variability on surface ozone during the NEAQS (2002) and ICARTT (2004) field campaigns. *J. Geophys. Res.*, **112**, D10S14, doi:10.1029/2006JD007590.
- Wolfe, D. E., and Coauthors, 2007: Shipboard multi-sensor merged wind profiles from New England Air Quality Study 2004. *J. Geophys. Res.*, **112**, D10S15, doi:10.1029/2006JD007344.
- Wulfmeyer, V. O., and T. Janjić, 2005: Twenty-four-hour observations of the marine boundary layer using shipborne NOAA high-resolution Doppler lidar. *J. Appl. Meteor.*, **44**, 1723–1744.
- , M. Randall, W. A. Brewer, and R. M. Hardesty, 2000: 2 μm Doppler lidar transmitter with high frequency stability and low chirp. *Opt. Lett.*, **25**, 1228–1230.